





Distribution, Sources, and Dynamics of Particulate Matter Along Trans-Arctic Sections

Wilford D. Gardner¹ , Mary Jo Richardson¹, Alexey V. Mishonov² , Phoebe J. Lam³ , and Yang Xiang¹ 

¹Department of Oceanography, Texas A&M University, College Station, TX, USA, ²CISESS/ESSIC/University of Maryland, Silver Spring, MD, USA, ³Department of Ocean Sciences, University of California, Santa Cruz, CA, USA

Special Section:

Uncovering the hidden links between dynamics, chemical, biogeochemical and biological processes under the changing Arctic

Key Points:

- First trans-Arctic section of beam attenuation (c_p) and Chl- a concentrations reveals significant interaction with Arctic hydrography on a basin scale
- Optical proxies for particle mass, particulate organic carbon, and Chl- a enable general identification of particle sources and dynamics
- Nepheloid layers are evidence of sediment transport from margins to basins and their limited presence in deep basins indicate weak currents

Correspondence to:

W. D. Gardner,
wgardner@ocean.tamu.edu

Citation:

Gardner, W. D., Richardson, M. J., Mishonov, A. V., Lam, P. J., & Xiang, Y. (2022). Distribution, sources, and dynamics of particulate matter along trans-Arctic sections. *Journal of Geophysical Research: Oceans*, 127, e2021JC017970. <https://doi.org/10.1029/2021JC017970>

Received 31 AUG 2021
Accepted 4 JUN 2022

Abstract In order to better understand the sources, sinks, and hydrodynamic influences on particulate matter distribution and variability in Arctic basins, we combined transmissometer data from two 2015 fall expeditions: one from Bering Strait (USCGC Healy) and the other from Barents Sea (R/V Polarstern) meeting at the North Pole. These first trans-Arctic sections of beam attenuation were overlain by salinity, temperature, and chlorophyll- a fluorescence (Chl- a) contours. Chl- a sections were overlain by nitrate contours. Particle composition analyzed from filtered samples throughout the full water column aided significantly in discerning sources, distribution, and dynamics of particles. Dense Pacific water moving swiftly through Bering Strait erodes and carries sediment-laden waters onto the Chukchi Shelf and into the Canada Basin. This nutrient-rich Pacific water sinks below a low-salinity, nutrient-poor polar mixed layer, forming a thick lens of high salinity water known as Pacific halocline water (salinity 31–33). Ice and the nutrient-poor mixed layer inhibit photosynthesis in surface waters of Canada and Makarov Basins, but subsurface chlorophyll- a maxima are observed if nutrients and light are available. Surface-water biomass is greater in the Barents Sea than in the Beaufort Gyre because nutrient-rich Atlantic water entering Barents Sea is not isolated from surface waters by ice or strong stratification. Surface water cools, creating high-density water that cascades into ~400 m basins in Barents Sea and into deep Nansen Basin, eroding sediment that creates patches of nepheloid layers in the shallow basins. Intense nepheloid layers in the deep basins are rare, suggesting weak bottom currents.

Plain Language Summary We combined optical data from two 2015 fall expeditions meeting at the North Pole to create the first trans-Arctic section of beam attenuation to estimate particle distribution. High-resolution optical measurements of particle concentration throughout the water column were coupled with simultaneous measurements of salinity, temperature, chlorophyll- a fluorescence, and nitrate. Particle composition analyzed from filtered samples aided significantly in discerning sources, distribution, and dynamics of particles. Dense, nutrient-rich Pacific water comes through Bering Strait and sinks below a thin, low-density, low-nutrient surface mixed layer, forming a thick lens of higher salinity water. Based on low chlorophyll concentrations in nutrient-poor surface mixed layers, surface-water photosynthesis is likely inhibited in some areas, but subsurface chlorophyll- a maxima are observed when nutrients and sufficient light are available. Nutrient-rich Atlantic water enters the Barents Sea, fueling high surface chlorophyll- a concentrations. Surface water cools, forming high-density water that cascades into ~400 m basins in Barents Sea and into Nansen Basin, eroding sediments that form patches of turbid layers (nepheloid layers) along slopes and in shallow basins. Intense bottom nepheloid layers in the deep basins are rare, suggesting weak bottom currents.

1. Introduction

Because of seasonal to year-round ice cover, the Arctic waters have been studied less than other oceans (Seidov et al., 2015). Global warming is shrinking the ice cover, making the Arctic waters more accessible. Technological advances in icebreakers and instrumentation plus international collaboration have enabled significant expansion of exploration and discovery in the Arctic Ocean in recent decades. Further motivation for understanding conditions in the Arctic Ocean comes from existing and developing plans to extract hydrocarbons from beneath the Arctic Ocean seafloor, and to access shorter shipping routes between the North Atlantic and Pacific oceans via previously inaccessible passages. Understanding the impact of increased human activity in the region requires that we record, monitor, and understand present conditions and natural processes in order to predict, measure, and assess future impacts.

For the purpose of understanding sediment transport in the deep Arctic basins, Hunkins et al. (1969) collected nephelometer profiles (Thorndike & Ewing, 1967) through the water column to the seafloor while drifting on ice camps from Canada Basin, northwest to the Mendeleev Ridge and then north across Alpha Ridge. Only weak nepheloid layers were observed and most profiles in Canada Basin had no benthic nepheloid layer. Sampling methods have improved tremendously since the early nephelometer era. Jackson et al. (2010) used optical transmissometers and fluorometers to study the distribution of PM and Chl-*a* in the upper 600 m along shelf-slope sections of the Canada Basin from 2003 to 2008.

Other Arctic studies have provided evidence of lateral sediment transport from the Chukchi Shelf and slope to the Canada Basin based on sediment trap studies (Honjo et al., 2010; Hwang et al., 2015; O'Brien et al., 2013) or vertical sampling of water in those regions (Xiang & Lam, 2020). Eddy transport can contribute to the transfer of water, sediment, and nutrients from the Chukchi Shelf to the Beaufort Gyre (Kadko et al., 2008; Kipp et al., 2018; Mathis et al., 2007; Spall et al., 2008; Watanabe et al., 2014), and play an important role in Arctic circulation (O'Brien et al., 2013; Timmermans & Marshall, 2020).

We analyzed and present here a trans-Arctic section of beam attenuation measured by transmissometers. These optical data, usually recorded at 10 Hz, were reduced to 2 db vertical resolution. Transmissometer data have been used globally to determine the distribution of particulate matter (PM) and particular organic carbon (POC) throughout the water column (Bishop & Wood, 2008; Boss et al., 2015; Gardner, Biscaye, Zaneveld, & Richardson, 1985; Gardner, Richardson, & Mishonov, 2018; Gardner, Richardson, Mishonov, & Biscaye, 2018; Mishonov et al., 2003). PM measured with transmissometers can serve as a non-conservative, short-term tracer that can shed light on multiple processes occurring within the ocean; for example, introduction of particles via rivers, PM distribution, and resuspension/transport of bottom sediments.

In this paper, we aim to improve understanding of conditions across Arctic basins by combining concentrations of PM measured simultaneously by transmissometry together with chlorophyll-*a* fluorescence (Chl-*a*), temperature, salinity, and nitrate along basin-wide transects of two simultaneous expeditions to the North Pole, coming from opposite sides of the Arctic Ocean performed in mid-August - early October of 2015. Combining those data with measurements of particle composition sampled by full depth, in situ large-volume filtration by Xiang and Lam (2020) during one of the cruises provides valuable information about the composition and distribution of PM throughout the Arctic section. Optical measurements of chlorophyll-*a* fluorescence help to identify biomass in surface waters and subsurface chlorophyll-*a* maxima (SCM) and conditions that favor SCMs. Combining compositional measurements of PM and Chl-*a* helps to identify their first-order source (biogenic vs. terrigenous) throughout the water column. Some of the questions we address are: How are particle distributions influenced by Arctic hydrography? How do optical proxies for particle mass, POC and Chl-*a* aid in identifying particle sources and dynamics? Is sediment transported from Arctic shelves to the inner basins? What differences are there in particle sources and dynamics between the Pacific and Atlantic regions of the polar transects? Where are subsurface chlorophyll maxima found in the Arctic Ocean? Are there benthic or intermediate nepheloid layers that indicate resuspension of shelf, slope, or deep basin sediments?

2. Background: Arctic Ocean Hydrography

Detailed descriptions of the seasonal and regional hydrography and currents of the Arctic Ocean can be found in Jones (2001), Rudels et al. (2004), Seidov et al. (2015), Steele et al. (2004), and Timmermans and Marshall (2020). These authors documented how the Arctic Ocean is fed from both the Pacific (inflow rate ~ 1 Sv) and Atlantic (inflow rate ~ 9 Sv) oceans, with water exiting only to the North Atlantic along several routes (Figure 1).

Sediment and abundant nutrients from the Yukon River join with Pacific water and move north into the Arctic Ocean through the 40–50 m deep Bering Strait (Jones et al., 2003; Nelson & Creager, 1977; Roach et al., 1995). Pacific water density is greater than the low-salinity surface polar mixed layer that contains fresher water from annual melting of sea ice plus fresh water outflow from Arctic rivers such as Canada's Mackenzie River, and several rivers from the Siberian Sea along northern Russia (Kipp et al., 2018). Most of the Pacific water sinks beneath the polar mixed layer as it moves off the Chukchi Shelf, forming a thick lens of high salinity water ($31 < S < 33$) that is known as Pacific halocline water (Steele et al., 2004). Pacific halocline water rests on top of the denser Atlantic water entering through the eastern side of Fram Strait and through the Barents Sea in the eastern Arctic Ocean. The deepest connection to or from the Arctic is Fram Strait with maximum depth of 2,600 m

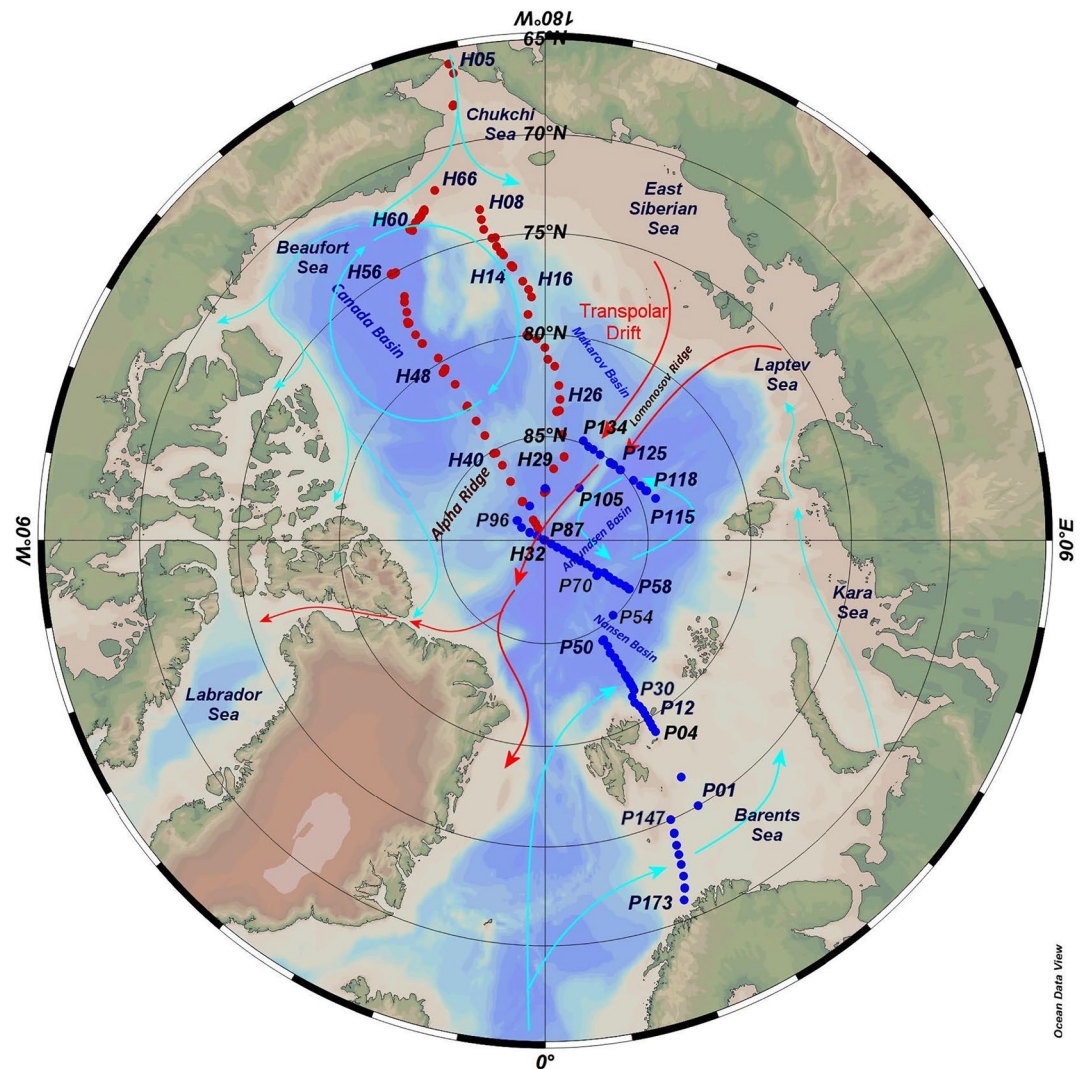


Figure 1. Map of Arctic Ocean and major circulation patterns with station positions of the USCGC Healy (from H05 to H66, red dots) and R/V Polarstern (from P01 to P173, blue dots). The large gyre next to the Beaufort Sea overlapping with most of stations during the USCGC Healy cruise is the Beaufort Gyre. Light blue arrowed lines indicate general surface flow or circulation. Red arrowed lines indicate general flow of the Transpolar Drift (flow lines after Charette et al., 2020).

and width of 450 km where cooler, fresher water in the western strait flows south, while warmer, saltier water in the eastern strait flows north (Timmermans & Marshall, 2020). The above studies emphasize that in the cold water of the Arctic Ocean, salinity is the major factor controlling the water mass density, not temperature, as is the case at lower latitudes.

Sea ice covers most of the Arctic Ocean in winter, though much of the Barents Sea is ice-free year-round. The areal extent of permanent sea ice has diminished significantly in recent years, causing changes in hydrologic and biological cycles (Katlein, et al., 2015; Perovich et al., 2019). By August there is no ice cover in the Barents Sea out to the edge of the Nansen Basin (Fetterer et al., 2017). Over on the Pacific side of the Arctic Ocean, winds, tides, and currents move Pacific Ocean water through the Bering Straits, melting annual ice and pushing ice out of the Chukchi Sea and into the Beaufort Gyre in the summer and fall.

Several studies have sought to unravel how the Pacific water crosses the Chukchi Shelf. Timmermans and Marshall (2020) state that a major portion of the water coming through Bering Strait moves through or above Barrow Canyon. Spall et al. (2018) identify three key locations where the transport occurs: Barrow Canyon, the Beaufort shelf break, and the Chukchi Shelf break and slope, with most of the water eventually passing

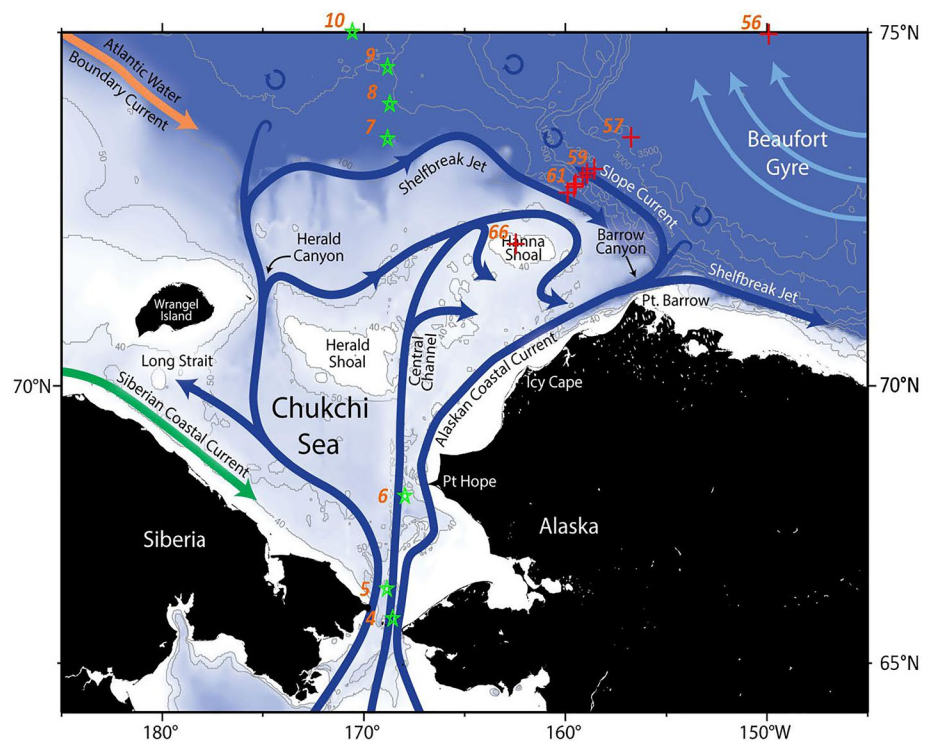


Figure 2. Stations along the trans-Arctic transect (red pluses; corresponds to Figure 5) and semi trans-Arctic transect (green stars; corresponds to Figure 6) overlain on a bathymetric map showing the schematic circulation in the Chukchi Sea and western Arctic Ocean (modified from Corlett & Pickart, 2017).

through Barrow Canyon and then splitting to the west to form the Slope Current and to the east, forming the Shelfbreak Jet (Corlett & Pickart, 2017; Figure 2). It is a complicated system involving a wind-driven anticyclonic gyre and flow exiting Barrow Canyon that is driven partially by variable currents through Bering Strait (Spall et al., 2018). Flow up or down Barrow Canyon could persist for days at speeds as high as 100 cm s^{-1} , so it was not just tidally driven. The long-term mean velocity was directed down canyon at $15\text{--}20 \text{ cm s}^{-1}$ (Aagaard & Roach, 1990; Mountain et al., 1976; Woodgate et al., 2005). Tidal fluctuations in up-down canyon flow have been observed in other submarine canyons where both currents and beam c_p were measured simultaneously (Gardner, 1989; Hunkins, 1988; Puig et al., 2013), resuspending and moving sediment seaward as intermediate nepheloid layers. Field studies using current meters, transmissometers, Chl-*a* fluorometers, and sediment traps off of the Mackenzie shelf ($\sim 500 \text{ km}$ east of Bering Strait), also showed occasional strong currents (100 cm s^{-1}) that resuspend carbon-rich shelf sediment and carry them out beyond the shelf into Canada Basin (Forest et al., 2007).

Satellite-derived eddy kinetic energy estimates show that shelf and shelf-edge boundary current regions have higher energy than the interior Canada Basin and Nordic Seas (Armitage et al., 2017). Narrow, seasonally varying boundary currents with typical speeds around 15 cm s^{-1} are trapped at the shelf breaks in the Nansen, Canada and Makarov Basins (Timmermans & Marshall, 2020). Speeds of $15\text{--}20 \text{ cm s}^{-1}$ at 1 m above the bottom will resuspend sediments along the shelf and basin margins (Miller et al., 1977, Figure 6), so sediment can be resuspended and moved seaward, but no currents of that intensity have been reported in the $\sim 4,000 \text{ m}$ deep basins.

Much of the Pacific Ocean water entering the Canada Basin is entrained in the wind-driven, predominantly anticyclonic flow of the Beaufort Gyre (Timmermans & Marshall, 2020). Circulation of Pacific water in the Beaufort Gyre and water from large rivers along East Siberia and Laptev Sea contribute to the wind-driven Trans-Polar Drift crossing the polar region (Spall et al., 2018) carrying sediment and nutrients as well as fresher water to the polar region (Kipp et al., 2018; Rutgers van der Loeff et al., 2018).

Radium-228 (a natural isotope formed from the decay of Th-232 and enriched in sediment pore waters) is found across the Chukchi Sea shelf and slope. Ra-228 can be released by diffusion or resuspension of sediment,

indicating that pore water nutrients and fine-grained sediment could also be transported beyond the shelf to the central basin (Kipp et al., 2018). Similarly, analysis of several parameters including dissolved organic carbon, Chromophoric Dissolved Organic Matter fluorescence, neodymium (Nd), and dissolved iron (dFe) demonstrated that the Trans Polar Drift moves water and nutrients from the Siberian rivers and shelf across the Arctic Ocean to the Canadian region, also passing over the polar area (Charette et al., 2020; Rutgers van der Loeff et al., 2018; Slagter et al., 2017, Figure 1). The point of departure of the Trans-Polar Drift from the East Siberian Sea shifts over time (Kipp et al., 2018). The Trans-Polar Drift water either continues circulating in the Beaufort Gyre (Figure 1, blue arrows) or exits the Arctic Ocean through the Canadian Archipelago or through the west side of Fram Strait (Rudels et al., 2004; Figure 1, red arrows).

3. Methods

Data presented in this paper come from simultaneous expeditions on two icebreakers: the U.S. GEOTRACES (GN01) [ARC01] Expedition on the USCGC Healy (Kadko & Landing, 2015) and the PS94 Expedition (GEOTRACES GN04) on the German R/V Polarstern (Ober et al., 2016a, 2016b; Rabe et al., 2016a, 2016b; Schauer, 2016). Both ships started their voyages in mid-August 2015, rendezvoused at the North Pole and at another station to sample simultaneously for inter-laboratory calibration of multiple sensors and parameters. Sampling continued from each ship along different routes back to their starting points, finishing in mid-October. We combined hydrographic and optical data from the two expeditions across the entire Arctic Ocean from the Bering Strait, across the Chukchi Shelf and Canada and Makarov Basins to the North Pole, and across Amundsen and Nansen Basins and the Barents Sea (Figure 1) to make a full water column, basin-wide section of beam attenuation due to particles, c_p . A second, shorter section is roughly parallel to the first one, beginning in the Bering Strait across Makarov and Amundsen Basins to the Gakkel seafloor spreading ridge.

Both ships were equipped with multiple CTD rosettes that included water collection bottles, WetLabs transmissometers, and either WetLabs or SeaPoint Chl-*a* fluorometers capable of reaching all depths in the Arctic Ocean. Xiang and Lam (2020) deployed a string of large-volume in situ filtration pumps (hundreds of liters filtered per depth) with a bottom-attached Seabird 19plus CTD/WetLabs transmissometer package during the USCGC Healy cruise. CTD rosettes on the Healy also had photosynthetically active radiation (PAR) sensors on many hydrocasts to estimate the depth of euphotic zones (Lee et al., 2007).

The transmissometer beam attenuation coefficient due to particles (c_p) and fluorescence-based Chl-*a* measurements from both ships were recorded in volts and analyzed by the TAMU/UMD-NCEI group using the factory calibrations in the same manner as in Gardner, Richardson, and Mishonov (2018). De-icing and cleaning transmissometer optical windows to obtain reliable air calibrations prior to each cast was not always possible in the Arctic because of freezing weather conditions. Without reliable air calibrations from all six transmissometers used on the two ships, the profile minimum signal found below 200 m from each deep-water cast for the open-ocean profiles, was set to zero. For stations with profiles less than 200 m depth a cruise-average minimum value calculated based on all deep-water profiles was used. The c_p data are reported in units of m^{-1} . Sections of c_p and other variables are gridded using the weighted-average method (ODV, Schlitzer, 2020) with search radii of about 40 km along the transect and 20 m vertically. Calibrated data from USCGC Healy expedition can be found at CCHDO data repository (expocode 33HQ20150809). Original data from R/V Polarstern can be found in PANGAEA data sets (http://doi.org/10.2312/BzPM_0703_2016 and <http://hdl.handle.net/10013/epic.48723>), with finalized data at <https://odv.awi.de/en/data/ocean/global-transmissometer-database/>.

During the USCGC Healy expedition, Xiang and Lam (2020) collected size-fractionated particles at 2–24 depth levels (depending on water depth and available ship time) at 20 stations using large-volume in situ pumps. Hundreds of liters of water are pulled through a 51 μm polyester mesh and then through either paired 0.8 μm Supor polyethersulfone or paired 1 μm quartz fiber filters to collect in situ size-fractionated (1–51 and >51 μm) particles. Major biogenic phases, including POC, biogenic silica (bSi), and CaCO_3 , were measured, as well as particulate aluminum (pAl) and particulate trace metals. PM was estimated as the chemical dry weight of the sum of all major particle phases in each size fraction. Refer to Xiang and Lam (2020) for a complete description and discussion of the size-fractionated particle composition and concentration during the GN01 cruise. Particle composition data are available through BCO-DMO and through the GEOTRACES Intermediate Data Product (2021).

All CTD packages were equipped with either a WetLabs (excitation/emission at 470/695 nm wavelengths) or SeaPoint (excitation/emission at 470/685 nm wavelengths) Chl-*a* fluorometer. The factory Scale and Dark values were used in standard SeaBird SeaSave software for data reduction and the data were recorded as fluorescence-based Chl-*a* ($\mu\text{g l}^{-1}$). Both manufacturers point out that their Chl-*a* fluorometers are calibrated with a monoculture of phytoplankton at the factory. The optical fluorometer measurements on the CTD provide much higher vertical and horizontal resolution than bottle data. Water samples were drawn from bottles in the upper 100 m for High-Performance Liquid Chromatography (HPLC) measurements at 27 Arctic GEOTRACES stations on the USCGC Healy. There were no HPLC measurements from the R/V Polarstern. Fluorometer Chl-*a* data from the two expeditions had a constant offset relative to each other with R/V Polarstern data having elevated values (about $0.015 \mu\text{g l}^{-1}$) compared to USCGC Healy data. This may have resulted from a difference in fluorometer brands, the phytoplankton species used for factory calibration, or the 10 nm difference in emission wavelength. To make Chl-*a* data from two expeditions comparable, we performed data adjustments similar to c_p data processing, using deep-water Chl-*a* minima as a reference point for each profile.

4. Results

Our data provide the first trans-Arctic section of c_p . We examine relationships among c_p , PM, POC, pAl, salinity, temperature, and Chl-*a*. One section crosses the entire Arctic Ocean and a second shorter section extends from the Chukchi Shelf to 85°N and then moves into the Amundsen Basin (Figure 1).

4.1. Relating Optical Signals to Particle Measurements

The optical measurements from transmissometry and fluorescence were compared to measurements of size-fractionated PM and POC collected by in situ filtration and pigments measured by HPLC collected by Niskin bottle filtration. It is not possible to differentiate the c_p from the two size fractions separately, so the total concentration of particles $>1 \mu\text{m}$ from the two size fractions is summed. The total weights were regressed against beam c_p (m^{-1}) from the USCG Healy expedition through the whole water column to estimate conversion factors between c_p and PM or POC (Figure 3). We use the term PM rather than suspended particulate matter or total suspended matter because unless the particles are in a surface or bottom turbulent mixing layer, there is no suspending force impeding the gravitational descent of particles.

Concentrations of PM differed by one to two orders of magnitude between shelf and open ocean regions. We separated the data into two groups based on location of stations for the USCGC Healy expedition where in situ filtration was conducted: those from the Bering Sea, Bering Strait, and Chukchi Shelf/Slope (stations H1–10 and H60–66, Figure 1), and those in the Canada, Makarov and Amundsen Basins (stations H11–H57, Figure 1) for regression analysis. Regression slopes for PM/c_p were $1768 \mu\text{g}\cdot\text{m l}^{-1}$ (shelf/slope) and $632 \mu\text{g}\cdot\text{m l}^{-1}$ (open ocean Canada, Makarov and Amundsen Basins), and for POC/c_p , $87 \mu\text{g}\cdot\text{m l}^{-1}$ (shelf/slope) and $238 \mu\text{g}\cdot\text{m l}^{-1}$ (open ocean Canada, Makarov and Amundsen Basins) (Figure 3). For comparison, these PM/c_p slope values bracket the value of $1,208 \mu\text{g}\cdot\text{m l}^{-1}$ calculated and used in our previous work to convert c_p to PM concentrations for global mapping of PM distribution throughout the water column (Gardner, Richardson, & Mishonov, 2018).

4.2. Euphotic Zone Depth

The depth to which primary production is likely to occur is the depth at which light intensity is 1% of the light at the surface (Marra et al., 2014). For stations H26–56, PAR data yielded 1% light level at depths of around 80–100 m, which is much deeper than the 5–50 m deep polar mixed layer (Peralta-Ferriz & Woodgate, 2015; Toole et al., 2010). No PAR data were reported for stations H11–H25.

4.3. Estimating Chl-*a* From Fluorometers

Chl-*a* has become a universal parameter for estimating phytoplankton biomass (Bidigare et al., 2005; Roesler et al., 2017). Just as transmissometer beam attenuation depends on particle composition and size, so Chl-*a* fluorescence also changes with natural variations in phytoplankton carbon to Chl ratios of different species and plankton photo-acclimation conditions (Roesler et al., 2017). They also noted that point by point comparisons for paired HPLC and in situ factory-calibrated Chl-*a* fluorescence measurements yield large scatter due to the variability in plankton species, light intensity, and plankton in vivo activity unless the data sets are restricted spatially and/

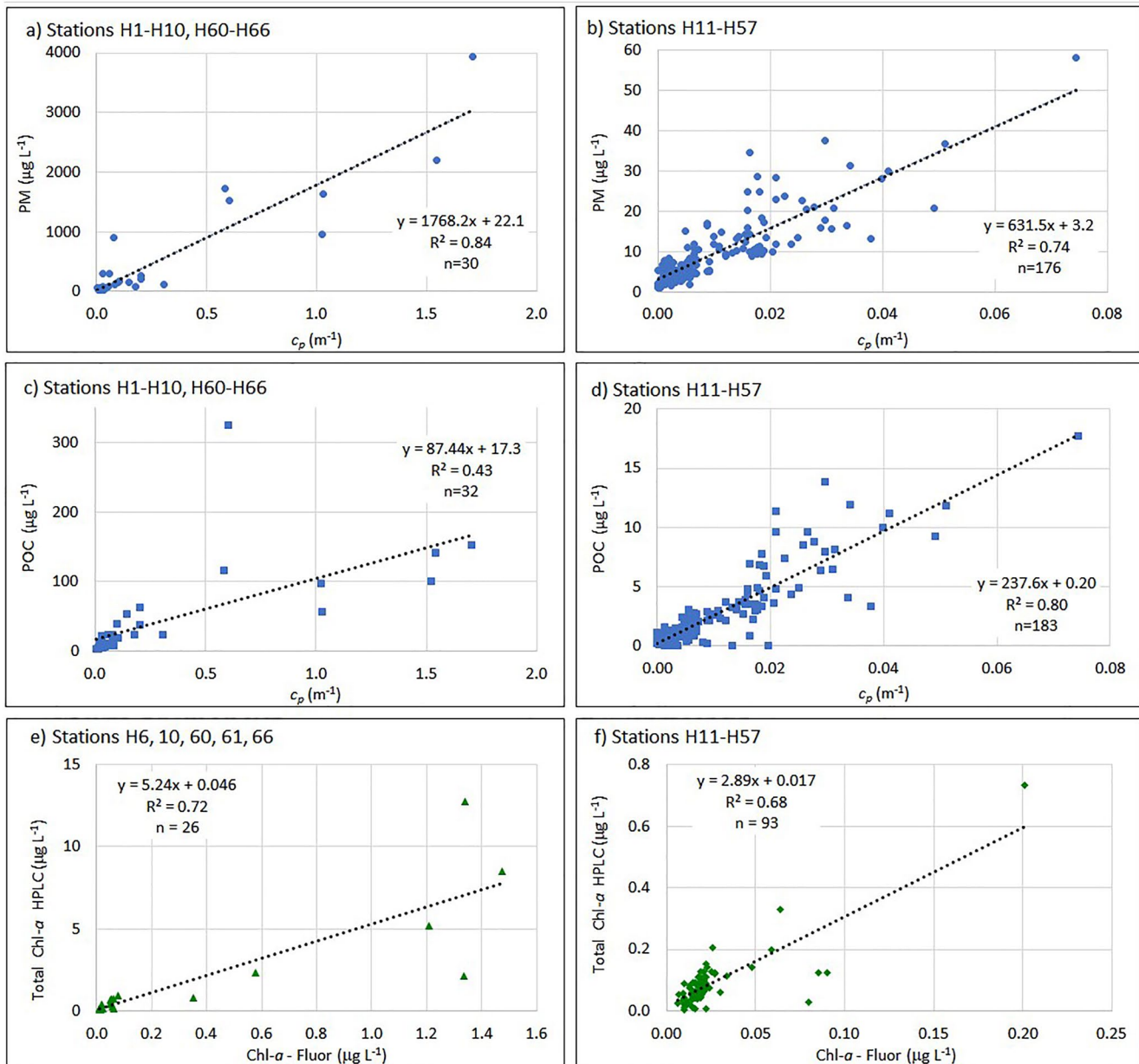


Figure 3. Linear regressions of c_p vs. (a) $> 1 \mu\text{m}$ PM sampled in the Bering Strait and shelf and slope of the Chukchi Sea, (b) $> 1 \mu\text{m}$ PM sampled in the open Arctic Ocean, (c) $> 1 \mu\text{m}$ particular organic carbon (POC) sampled in the Bering Strait and on the shelf and slope of the Chukchi Sea, (d) $> 1 \mu\text{m}$ POC sampled in the open Arctic Ocean. Note difference in scales. All PM and POC samples were analyzed by Xiang and Lam (2020). (e) Linear regression of HPLC Chl-*a* vs. fluorometer Chl-*a* on the shelf and slope, (f) linear regression of HPLC Chl-*a* vs. fluorometer Chl-*a* sampled in the open Arctic Ocean. Correlation is strong (~ 0.7 – 0.8) for all cases except for (c). Removing the single outlier point in (c) increases its R^2 to 0.82, and decreases slope to 77 and intercept to 12.4.

or temporally. They define the ratio between the factory-calibrated in vivo fluorescence-derived Chl-*a* and the HPLC-derived Chl-*a* as a dimensionless “slope factor”. This slope factor varies regionally between 1 and 6 for the major oceans they tested. Our slope factors are about 5 on the Chukchi Shelf/slope where conditions are highly variable and about 3 for the stations sampled in the open western Arctic ocean (Figures 3e and 3f).

4.4. Identifying Nepheloid Layers

Nepheloid layers were defined by Thorndike and Ewing (1967) as a cloudy layer caused by increased particle concentrations near the seafloor, not a specific concentration, due most likely to resuspension and advection of

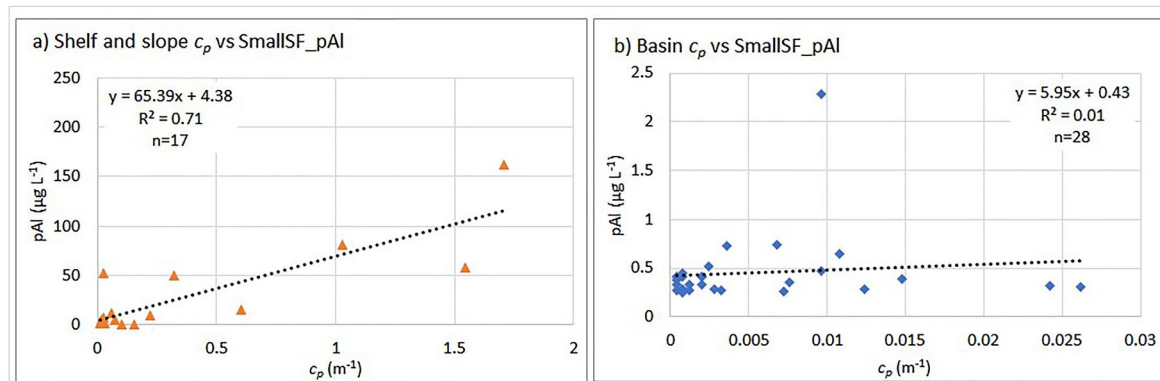


Figure 4. Linear regressions of c_p vs. pAl ($\mu\text{g l}^{-1}$) in the small size fraction (1–51 μm) on (a) the shelf and slope of the Chukchi Sea (stations H6–10 and H60–66), (b) in the open Arctic Ocean (stations H14–57). Only samples defined as benthic nepheloid layers in the Arctic basin (pAl > 9 nM [$0.24 \mu\text{g l}^{-1}$]; Xiang & Lam, 2020) are plotted.

bottom sediments. Intermediate nepheloid layers are caused by sediment resuspended by currents or by cascading of denser water down a slope and advection away from the slope (McCave, 1986). Transmissometer measurements with a CTD provide 2 db profiles throughout the water column. This allows high resolution in c_p , but does not give information about particle composition.

An alternative way to identify nepheloid layers is by the measurement of near-bottom increases in the concentrations of filtered particulate components. For example, Xiang and Lam (2020) measured numerous components of filtered material in the Arctic collected during this expedition and used the concentration of pAl as a sensitive indicator of stations that exhibited a near-bottom increase in lithogenic particles, indicating resuspension of near-bottom aluminosilicate sediments. They defined a nepheloid layer as water where pAl concentration is > 9 nM in the small size fraction (SSF: 1–51 μm) of filtered particles, equivalent to $0.24 \mu\text{g l}^{-1}$ pAl or $3.0 \mu\text{g l}^{-1}$ of lithogenic particle mass, assuming an upper continental crust Al composition of 8.04 wt% (Taylor & McLennan, 1995). To compare the optical and geochemical approaches of defining nepheloid layers, we plot the relationship between c_p and pAl in Figure 4. Unlike the comparisons of c_p with PM and POC (Figure 3), there is only a correlation between c_p and pAl in pAl-defined nepheloid layers at shelf/slope stations, and no correlation at basin stations.

We use data on the pAl of particles 1–51 μm because the c_p response comes mostly from particles 1–20 microns and is less sensitive to particles >40 microns (Boss et al., 2015, 2009; Gardner et al., 1993). On average, the SSF pAl constitutes $\sim 80\%$ of the total pAl (Xiang & Lam, 2020). At shelf stations, an average of 67% of the pAl comes from the SSF and in off-shelf stations the SSF makes up 90% of the pAl.

4.5. Relationships Between c_p , Salinity, Temperature, and Chl-*a* Along Trans-Arctic Sections

The c_p values along the trans-Arctic sections are shown by the color scales in Figures 5 and 6. The same color bar for c_p is used for 0–500 m in all sections. Due to the low PM concentrations in deeper water, a more sensitive color bar range for c_p is used for water depths greater than 500 m in Figures 5a and 6a to more accurately show benthic nepheloid layers.

Contours of salinity, temperature, and Chl-*a* are overlain on the c_p sections. c_p can be converted to PM or POC using the equations in Figure 3. USCGC Healy ship logs indicate ice thickness along the Healy track was generally ~ 1 –2 m and along R/V Polarstern track average ice thickness was about 1.6 m (Schauer, 2016, Figure 4, 5). The presence/absence of ice based on those two sources is schematically indicated at the top of Figures 5–7. The Chukchi Shelf and Barents Sea were both ice free during time of sampling. Sea ice coverage increased from 20% to 80% moving across the Canada Basin. Pack ice covered Markov, Amundsen and most of Nansen basins (Figures 5a and 6a). Particle concentrations based on c_p were highest in the Bering Strait, on the Chukchi Shelf, and in the Barents Sea, especially in ice-free areas. Lower salinity, colder Pacific water enters through the Bering Strait and saltier, warmer water (up to 8°C) enters from the Atlantic, cools and sinks below the Pacific water. In the Chukchi Sea, intermediate nepheloid layers extend offshore from the shelf and from several depths down to

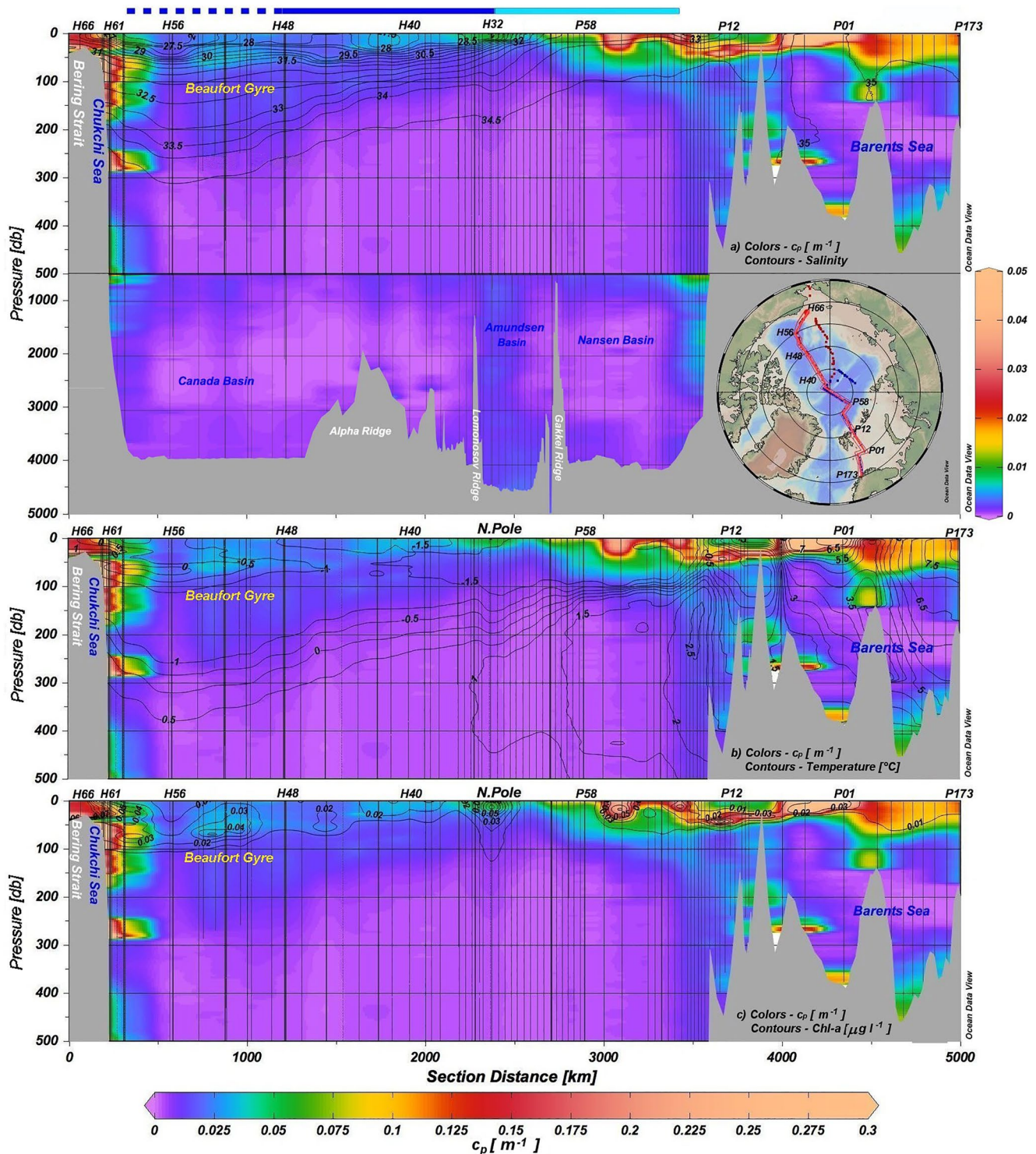


Figure 5. Sections of c_p from Bering Strait via North Pole to Norway with contours of (a) salinity, (b) seawater temperature, $^{\circ}\text{C}$, and (c) fluorescence-based Chl- a , $\mu\text{g l}^{-1}$. Note the y-axis (pressure) scale change at 500 db (panel (a)). Color scale is c_p (m^{-1}) (a proxy for PM or POC, see Figure 3), and shown as a horizontal color bar beneath the sections for 0–500 m panels (a–c) and as a short vertical color bar on the right-hand side of the deep portion of panel (a) for water >500 m. The finer scale is to better visualize the benthic nepheloid layers in the deep basins. Blue lines above the sections schematically represent the sea surface ice condition: dashed line indicates the area along which ice cover increased from 20% to 80%, bold blue line represents area covered by >80% ice, light-blue line indicates ice-covered area reported by Schauer (2016; figure 4.5) for the R/V Polarstern expedition. No line represents relatively ice-free areas. Vertical dotted lines are station locations and the labels above each frame are station numbers (*H* for Healy, *P* for Polarstern). Some station lines appear thicker because multiple casts were made there. The cruise map in the top panel indicates the stations along orange lines used in this section. Distance along ship track is used for the x-axis. Note the y-axis (pressure) scale change at 500 db (panel (a)).

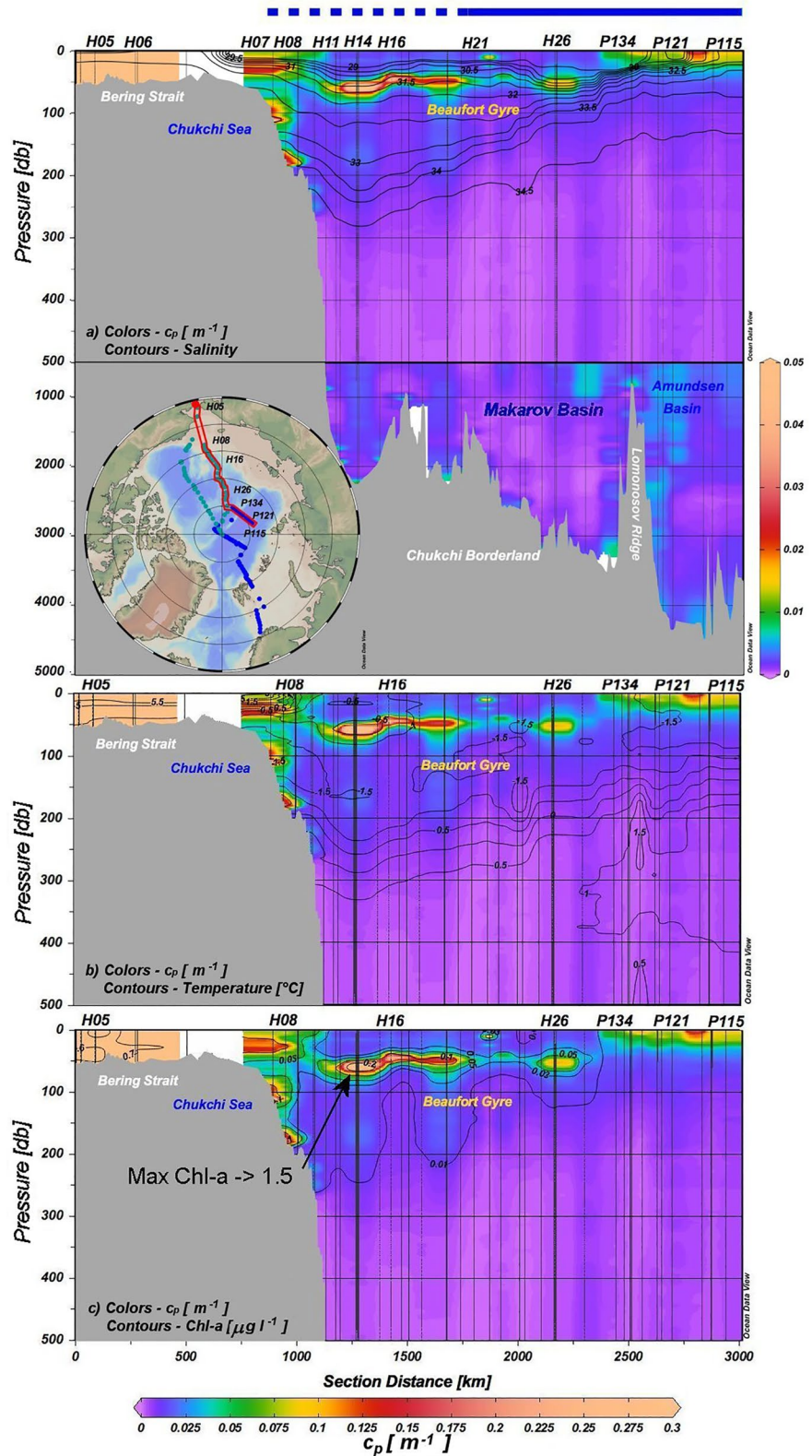


Figure 6. The semi trans-Arctic section (see green line on map inset) of c_p (color scale) from Bering Strait to Amundsen Basin (Northbound) with contours of (a) salinity, (b) seawater temperature, $^{\circ}C$, and (c) fluorescence-based Chl-a in $\mu g l^{-1}$. y-axis and color bars as for Figure 5; see Figure 5 caption for details.

at least 500 m, indicating transport from the shelf/slope into Canada Basin. In the small basins of the Barents Sea there were intermediate and benthic nepheloid layers between 300 and 450 m (Figure 5).

Temperature and salinity contours align well with c_p distribution in Canada through Amundsen Basins for both transects (Figures 5a, 5b, 6a, and 6b). There is higher c_p in the Pacific Halocline water (salinity 31–34.5) than in the Atlantic water in the central Arctic. Contours of Chl-*a* are extremely well aligned with the c_p distribution in surface waters of Nansen Basin, Makarov Basin, and Barents Sea (Figures 5c and 6c), suggesting a large portion of the c_p signal is from biogenic material in those areas except between stations P115–P134 (Figure 6c). The lack of Chl-*a* in that surface area of high c_p (Figure 6c) could be an impact of the Trans-Polar Drift bringing either lithogenic particles from the Siberian region (Charette et al., 2020; Kipp et al., 2018; Rutgers van der Loeff et al., 2018; Slagter et al., 2017, Figure 1) or old detrital POC that no longer contains fluorescent material.

High Chl-*a* seldom extended deeper than 100 m in either transect. On the southward transect (Figure 5c) none of the intermediate nepheloid layers between 100 and 500 m had Chl-*a* > 0.01 $\mu\text{g l}^{-1}$, indicating that the deeper layers were predominantly resuspended inorganic sediments, possibly entrained by the Slope Current or washed out through Barrow Canyon. On the northward transect (Figure 6c) across the Chukchi slope, Chl-*a* contours (>0.02 $\mu\text{g l}^{-1}$) match the c_p increases at 100 and 180 m. Chl-*a* also dipped down to more than 200 m well away from the shelf beneath two segments of high Chl-*a*, at 50 m depth.

In order to evaluate the relationship between Chl-*a* and nitrate distribution, we created two sections of Chl-*a* concentration to a depth of 200 m, overlain by contours of nitrate concentration and the mixed layer depth (Figure 7, dotted white line). Chl-*a* maxima were seldom observed near the surface, and only when nitrate

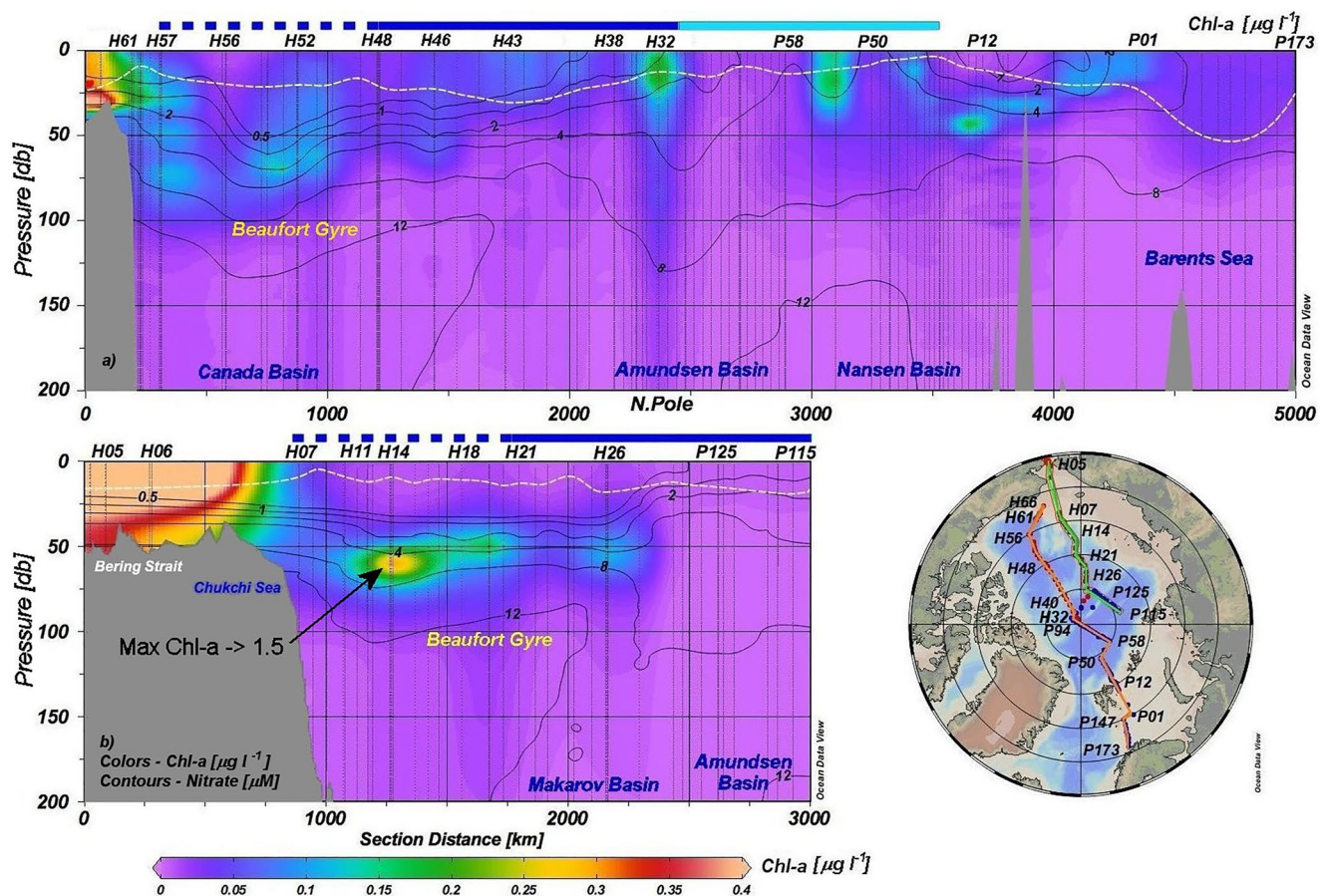


Figure 7. Sections of fluorescence-based Chl-*a* ($\mu\text{g l}^{-1}$) in color scale with black contours indicating nitrate concentrations (μM) for: (a) trans-Arctic section (orange line on map), and (b) semi trans-Arctic section (green line on map). Dashed white lines represent mixed layer depth estimated following Lorbacher et al. (2006), as the depth of the second derivative maximum of the density profile closest to the surface. Blue lines at the top schematically represent the sea surface ice condition as described in Figure 5 caption.

concentration was greater than 0.5 μM . Subsurface maxima occurred along the two transects. Most notable is the maximum of 1.5 $\mu\text{g l}^{-1}$ at station H14 recorded during several casts performed at this location (Figure 6c).

5. Discussion

5.1. Effect of Particle Composition on PM/c_p Relationship

It is not just total PM concentration that determines the variation in PM/c_p slopes, but also particle composition. PM is comprised of a mixture of different particle components, such as particulate organic matter (POM), CaCO_3 , biogenic silica, and lithogenic particles, each of which may have different optical properties. Here we examine the sensitivity of c_p to PM and to two components of PM; POM, traced by POC, and lithogenic particles, traced by pAl. Xiang and Lam (2020) estimated the mass of POM and lithogenic particles in these Arctic waters by using a factor of 1.88 g of POM per g of POC based on nuclear magnetic resonance determinations of plankton composition (Hedges et al., 2002). To estimate the pAl concentration in lithogenic material collected, they used a factor of 0.08 g of pAl/g of lithogenic material based on average pAl concentrations in upper continental crust (Taylor & McLennan, 1995), which is the original source of lithogenic material. With these conversions, the shelf/slope region have POM/c_p and lithogenic particles/ c_p relationships of 164 $\mu\text{g POM-m l}^{-1}$ and 813 $\mu\text{g lithogenics-m l}^{-1}$. Given that a greater mass of lithogenic particles is needed to attenuate the beam compared to POM, a high abundance of lithogenic particles increases the observed PM/c_p regression slope. The high PM in the Chukchi Shelf/slope regions of the Arctic Ocean was predominantly caused by resuspended lithogenic particles, accounting for >50% of PM (Xiang & Lam, 2020). Lithogenic particles dominate high PM on the shelf, but are a small component of PM in the basin. This explains why the PM/c_p slopes are so different between the shelf/slope and basin (Figure 3). The smaller regression slope of POC/c_p compared with PM/c_p in both shelf/slope and open ocean environments in the Arctic Ocean (Figures 3a–3d) indicates that a change in c_p reflects a smaller change in POC than in PM.

In reality, there is no globally applicable slope for such regressions because of natural variations in particle composition and size. In regions of the ocean where POC is the dominant component of PM, the POC/c_p relationship may be fairly constant (Bishop & Wood, 2008). The PM/c_p relationship varies as a function of particle size, shape, and composition (Baker & Lavelle, 1984; Boss et al., 2015; Gardner, 1989), which varies with depth. For this reason, we plot beam c_p in units of m^{-1} rather than applying a single conversion factor to obtain PM or POC. As a rough estimate drawn from these plots, a 0.1 m^{-1} increase of c_p is approximately equal to 177 $\mu\text{g l}^{-1}$ increase in PM on the shelf and 63 $\mu\text{g l}^{-1}$ in the open Arctic Ocean. For POC, a 0.1 m^{-1} increase of c_p is equal to approximately 9 $\mu\text{g l}^{-1}$ increase on the shelf and 24 $\mu\text{g l}^{-1}$ in the open Arctic Ocean.

5.2. Processes Controlling PM (c_p) and Chl-*a* Distribution in the Upper 500 m of the Arctic Ocean

In the eastern Arctic, Atlantic water entering through the Barents Sea encounters irregular bottom topography (vertical scales highly exaggerated in all figures) including small basins ranging in depth down to 450 m. Much of the Barents Sea has no seasonal ice cover, especially south of Svalbard (Timmermans & Marshall, 2020, Figure 2b), and strong winds during winter storms quickly cool the relatively warm (up to 8°C), salty (>35) water, some of which cascades down into these small basins, eroding sediment along the way (Figure 5; Ivanov et al., 2004), or into the Arctic basin beneath the Pacific water starting in the Nansen Basin and spreading across the Arctic Ocean.

Some of the highest rates of primary production in the Arctic Ocean are in the Chukchi and Barents Seas, and lowest primary production is in the central Arctic Ocean (Codispoti et al., 2013; Springer & Mcroy, 1993). Our data (Figures 5 and 6) are consistent with those studies in that the highest surface c_p and Chl-*a* values are recorded in the Chukchi Shelf/Sea and Barents Sea, especially in ice-free areas. Assuming that c_p in the eastern Arctic basins has a similar relationship with POC and PM as in the western Arctic basins (Figure 3), optically derived PM concentrations in surface waters are up to eight times greater in the Chukchi Shelf and Sea, Nansen Basin and Barents Sea (maximum c_p of 0.25 m^{-1}) than in most of the Canada Basin (maximum c_p of 0.03 m^{-1} , Figure 5a).

In Arctic surface waters, PM concentrations measured from the pump samples ranged between 10 and 100 $\mu\text{g l}^{-1}$, whereas in benthic nepheloid layers in the Bering Strait and on the Chukchi Shelf and upper slope, PM concentrations ranges increased ten-fold to 100 to >1,000 $\mu\text{g l}^{-1}$ (Xiang & Lam, 2020) and Figures 3a and 3b.

PM decreased with depth in all basins reaching minimum concentrations of about 1–7 $\mu\text{g l}^{-1}$ at around 2,000 m from in situ pump filtration (Xiang & Lam, 2020), which is comparable to clear water minimum concentrations in the GA03 North Atlantic cruise ($\sim 5 \mu\text{g l}^{-1}$) or in the GP16 Eastern Tropical South Pacific cruise ($\sim 4 \mu\text{g l}^{-1}$) estimated by the same methods (Lam et al., 2018; Lam, Ohnemus, et al., 2015; Lam, Twining, et al., 2015). The lower range of the minimum concentrations could result from lower surface primary production in ice-covered waters, as suggested by Honjo et al. (2010).

Abundant Chl-*a* was present on the Chukchi Shelf in the regions of high c_p . Low Chl-*a* was associated with small intermediate nepheloid layer intrusions of high c_p on the upper slope between about 50 and 100 m (Figure 5c), however, Chl-*a* was not found in turbid layers deeper than 100 m. Particles in the intermediate nepheloid layer at station H61 (Figure 5c) were characterized as 70% lithogenic material, with the remainder divided between opal ($\sim 20\%$), POM ($\sim 7\%$), and Fe oxides ($\sim 3\%$; Xiang & Lam, 2020), indicating resuspended particles were composed primarily of lithogenic material with some aged biogenic and authigenic material.

Using $\delta^{13}\text{C}$ -POC and a two end-member mixing model, Xiang and Lam (2020, figure 7) estimated that the small size fraction of POC below 100 m depth in the western Arctic basin is comprised of a mixture of vertically settling and laterally transported POC. Even in the middle of the basin, they estimated that up to 40% of POC is from lateral advection, which is consistent with observations made by others using sediment traps (Honjo et al., 2010; Hwang et al., 2015; O'Brien et al., 2013).

Our sections show the maximum lower Pacific halocline water depth (salinity >34.5) was at ~ 300 m at stations H56 (Figure 5a) and ~ 270 m at H14 (Figure 6a) and shoaled upward toward Barents Sea (Figures 5a and 6a). The deep penetration of particles in both the Canada (Figure 5) and Makarov (Figure 6) Basins coincides with the bottom of the lower Pacific halocline water. Particulate chemical tracers, including $\delta^{13}\text{C}$ -POC, MnO_2 , and elevated biogenic Si point to a shelf origin of particles found in the upper and lower Pacific halocline layers in the Canada and Makarov Basins (Jensen et al., 2020; Xiang & Lam, 2020), suggesting that the elevated c_p signal down to the bottom of the lower Pacific halocline water might be at least partly derived from lateral transport from the shelf/slope, with exact mechanisms of transport (e.g., internal waves [Cacchione & Drake, 1986] or eddies [Spall et al., 2008; Watanabe et al., 2014]), requiring further research.

5.3. Subsurface Chl-*a* Maxima

Chlorophyll maxima usually occur in surface waters, but Subsurface Chl-*a* Maxima (SCM) have been observed regularly in the Arctic Ocean as well as in stratified regions of all oceans (Ardyna et al., 2013; Cullen, 2015; Steiner et al., 2016). Arctic SCMs develop in the summer after the water column becomes stratified and surface nutrients are consumed. The SCM also acts as a boundary that prevents upward diffusion of nitrate into surface waters (Mundy et al., 2009; Tremblay et al., 2008). The low-density polar mixed layer and pack ice strongly inhibit upward mixing of nutrient-rich halocline waters with surface waters. The polar mixed layer thickness is typically 25–50 m in winter and 5–30 m in summer (Peralta-Ferriz & Woodgate, 2015; Toole et al., 2010).

SCMs are found along both sections except in the Barents Sea. In both sections (Figures 5c, 6c, and 7b) we observe SCMs of varying intensity between about 30 and 70 m depth, most notably in the Beaufort Gyre where the maximum Chl-*a* reached 1.5 μM and in the margin of the Nansen Basin (Figure 6c). c_p values are closely aligned with the elevated chlorophyll-*a* contours in Canada and Makarov Basins. Nitrate concentrations in the mixed layer in those two basins were usually less than 0.5 μM , but were between 0.5 and 4 μM in the Nansen Basin and Barents Sea (Figures 7a and 7b). Primary production in the Arctic and open ocean becomes limited when nitrate is below 0.5 μM (Henley et al., 2020; Landry et al., 1998). The low nitrate in the mixed layer plus light reduction due to sea ice could explain the low surface Chl-*a* and c_p in the strongly stratified western basins (Cai et al., 2010). We hypothesize that the higher values of nitrate in surface water of the eastern Arctic Ocean (including Barents Sea) results in higher Chl-*a* and c_p from primary production where there is more light available due to less sea ice cover (Figures 5c and 7a). PAR sensors on CTD hydrocasts yielded 1% light levels at around 80–100 m which is much deeper than the average mixed layer thickness (Figure 7, dotted white lines), therefore when nutrient concentrations exceed 0.5 μM , SCMs can develop at varying depths and intensities. There was insufficient nitrate for significant photosynthesis in surface waters between stations H07 and H26 and stations H40–H57 in the western Arctic, but sufficient nitrate and light for photosynthesis in patches of surface waters in the eastern Arctic (Figure 7a).

The SCM between stations H11 and H26 (Figure 6c) at about 50–70 m might be interpreted as advection of sediment and Chl-*a* from the shelf, but the high Chl-*a* values suggest that in situ primary production is a more likely source. No rates of primary production were measured during this expedition, but measurements of Ra-228 along both Healy transects show the presence of Ra-228 in the upper water column of central Arctic Basin which traces back to the Chukchi Shelf (Kipp et al., 2018, Figure S1). Kipp et al. (2019, 2020) state that the main source of Ra-228 in those regions is the shelf, including pore-waters from resuspended shelf sediments, and that shelf pore waters could also include nutrients moving into Canada Basin. The nutrient-rich water advected seaward by currents, internal waves (Cacchione & Drake, 1986), or eddies (Kadko et al., 2008; Kipp et al., 2018; Mathis et al., 2007; Spall et al., 2008; Watanabe et al., 2014), could enhance primary production of Chl-*a* along that pathway under proper conditions of light, nutrients and phytoplankton types. The Ra-228 layer is between ~50 and 200 m at station H54 (Kipp et al., 2018, Figure S1) and shoals up to 0–100 m by 85°N. The high Ra-228 layer vertically encompasses water deeper than the high Chl-*a* water, but 1% PAR only reaches 80–100 m deep, so Chl-*a* production would not be expected below that depth.

An unusual feature was observed near the North Pole, station 32 (Figures 5c and 7a). Surface salinity was <30 and the nitrate value from a surface bucket sample was zero. Salinity increased to 31 by 20 m depth. Nitrate was 2–4 μM between 20 and 60 m and continued increasing down to 200 m depth (Figure 7b). Chl-*a* reached a maximum of 0.2 $\mu\text{g l}^{-1}$ at 20 m, and decreased with depth down to 200 m in four separate profiles (all used in Figures 5c and 7a). Since 200 m is well below the euphotic zone, we hypothesize that some fresh phytoplankton was sinking to that depth before being consumed by grazing zooplankton. While traversing the gut of zooplankton, Chl-*a* is converted to pheophorbide and pheophytin (Strom, 1993) and would not add to the Chl-*a* signal. The Trans-Polar Drift moves water and nutrients from the Siberian rivers and shelf across the Arctic Ocean to the Canadian region, often passing over the polar region. We suggest that the water and components carried by the Trans Polar Drift are likely involved with this anomalous SCM (Charette et al., 2020; Kipp et al., 2018; Rutgers van der Loeff et al., 2018).

Both SCMs and surface Chl-*a* highs occur at varying depths in the upper 50 m in the Nansen Basin and Barents Sea along the Trans-Arctic section between 3,000 and 5,000 km (Figures 5c and 7a). Barents Sea had no ice cover, less stratified water, and in the eastern region a thicker mixed layer as deep as 50 m (Figure 7a, white dotted line), which allows deeper mixing, bringing subsurface nutrient-rich waters into the euphotic zone.

5.4. PM Distribution From c_p and Processes in the Barents Sea

Surface waters in the Barents Sea and Nansen Basin had Chl-*a* values similar to those in surface waters of the Canada, Amundsen, and Makarov Basins at this time of year (Figure 7a), but the surface c_p values were much higher in the Barents Sea and extended out to Nansen Basin. The tight match between Chl-*a* contours and c_p suggests a correlation of c_p with biomass concentrations in these surface waters. Conversely, the high values of c_p near the sides or bottom of small basins in the Barents Sea show no Chl-*a*, so those high c_p values are most likely due to lithogenic sediment being resuspended by cascading of cold, hypersaline water. c_p gradually decreases with distance from the Barents Sea/Nansen Basin border as well as with depth from the Barents Sea slope. Although the water entering Nansen Basin from the Barents and Norwegian seas is warmer than water from the Pacific, its salinity (>35), and therefore density (>27.5 g/cm^3), are greater than the Pacific water, so it sinks below the Pacific water as it spreads into the Arctic Ocean where it interleaves and mixes with colder water as seen in the temperature contours in Figure 5b.

5.5. PM Transport From Shelves to Deep Basins

Timmermans and Marshall (2020) noted that there are narrow, energetic, seasonally varying boundary currents, with typical speeds around 15 cm s^{-1} , trapped at the shelf breaks in the Nansen, Canada and Makarov Basins (see also Aksenov et al., 2011; Dmitrenko et al., 2016; Nikolopoulos et al., 2009; Pickart, 2004). Those speeds are sufficient to resuspend sediments (Miller et al., 1977). Depending on the wind strength, which is believed to drive the Slope Current off of Chukchi Shelf (Figure 2), strong currents could be found down to at least 40–125 m depth, however, they are not locked to a specific isobath and can wander (Corlett & Pickart, 2017). Velocity estimates from their figure 13 are about 20 cm s^{-1} . Figures 5 and 6 show some high concentrations of PM stretching

out 50–300 km offshore. Xiang and Lam (2020) found evidence of considerable lateral advection of lithogenic particles coming off the shelf based on particle composition.

Intermediate nepheloid layers with high PM concentrations appear in water bordering the Chukchi Sea between 100 and 600 m depth in both sections (Figures 5 and 6). PM concentrations in water coming out of the Bering Strait are 2,000–4,000 $\mu\text{g l}^{-1}$ in the bottom 30 m based on in situ filtered pump samples. Bering Strait water crosses the Chukchi Shelf and feeds the Alaska Coastal Current which moves off the Chukchi Shelf before it splits into the Shelfbreak Jet to the right (i.e., southeast) and the Slope Current to the left (i.e., northwest; Figure 2; Corlett & Pickart, 2017), which are likely one cause of the intermediate nepheloid layers in that area (Figures 5 and 6).

Another source of intermediate nepheloid layers could be Barrow Canyon. Many V-shaped canyons, like Barrow Canyon, experience strong up-down flows driven by tidal forcing that also resuspends sediment along its axis during flow in both directions, carrying resuspended sediment down the canyon until it reaches water of an equivalent fluid density (Gardner, 1989; Hunkins, 1988; Puig et al., 2013). At that point, the sediment-laden water detaches from the seafloor and moves seaward following that density interface, with sediment settling out along the way. This current oscillation can also occur along continental slopes (Cacchione & Drake, 1986) and could account for the high PM concentrations in water bordering the Chukchi Shelf in both sections (Figures 5 and 6). However, in contrast with currents reported in those North American east-coast canyons, up/down currents measured in Barrow Canyon were far less regular (Aagaard & Roach, 1990; Mountain et al., 1976; Spall et al., 2018; Timmermans & Marshall, 2020; Woodgate et al., 2005).

Off-shelf transport into the Canada Basin is well documented (Corlett & Pickart, 2017; Honjo et al., 2010; Jackson et al., 2010; O'Brien et al., 2013; Spall et al., 2018; Xiang & Lam, 2020). Long-term sediment trap deployments in Canada Basin off the Mackenzie shelf also confirmed off-shelf transport of sediment that decreased with distance from the shelf and was highly variable on an intra-annual time scale (O'Brien et al., 2013). They also noted the strong influence of cyclonic and anti-cyclonic eddies on sedimentation rates measured offshore. The pump data show off-shelf transport of large particles ($>51 \mu\text{m}$) as well as small particles ($<51 \mu\text{m}$; Xiang & Lam, 2020, Figures 3a, 4a, 7a, and 7c).

5.6. Benthic Nepheloid Layers in Arctic Basins

Benthic nepheloid layers are detected in Arctic basins by both optical and chemical measurements. Our optical data show nepheloid layers near the seafloor in the small basins of Barents Sea and near the continental margins in all Arctic basins. There are also areas in Canada, Amundsen and Nansen Basins where bottom PM concentrations are elevated based on c_p measurements (Figures 5a and 6a). Optical profiles provide high vertical resolution (2 db) of particle distributions throughout the water column, but lack the ability to assess particle composition.

Xiang and Lam (2020) observed near-bottom increases in particulate Al concentrations and used this to identify the presence and composition of benthic nepheloid layers in the Canada and Makarov Basins. Any near-bottom increase in lithogenic particle concentrations, however small, suggests that there must have been local resuspension of bottom sediments and/or the transport of sediments resuspended elsewhere. Coupling optical measurements with large-volume in situ filtration provides a powerful combination of techniques to better understand sources, sinks and dynamics of particles throughout the water column.

Based on a global compilation of benthic nepheloid layers, optically measured particle concentrations range from low ($10 \mu\text{g l}^{-1}$) to high ($100\text{--}1,000 \mu\text{g l}^{-1}$) with nepheloid layer thickness being meters to over a kilometer (Gardner, Richardson, & Mishonov, 2018; Gardner, Richardson, Mishonov, & Biscaye, 2018). The increase can result from local erosion and resuspension by currents, activity of benthic organisms, or accelerations of even weak currents among rough topography (Armi, 1978; Gardner, Southard, & Hollister, 1985; Gardner et al., 2016; McCave, 1986; Turnewitch et al., 2013). For nepheloid layers thicker than the benthic boundary layer vertical mixing ($\sim 10\text{--}100 \text{ m}$), the increase in PM must result from sediment resuspension along shallower seafloor followed by lateral advection by currents, or cascading of cold, dense water sinking and eroding/resuspending sediment.

The lowest total PM concentration from the large-volume in situ filtration in 2015 was in the range of 1–3 $\mu\text{g l}^{-1}$ in the clearest mid-water regions of the Canada Basin. Global measurements of PM concentration show a wide range of values in both surface and near-bottom waters. However, concentrations in the middle of the water column, that is, between ~ 200 m depth and a few hundred meters above the seafloor are generally less than about 5–12 $\mu\text{g l}^{-1}$ (Brewer et al., 1976; Gardner, Richardson, & Mishonov, 2018). Sufficient measurements have been made globally to map nepheloid layer characteristics such as maximum bottom concentration, integrated nepheloid layer mass and thickness for the major oceans. One of the findings was that nepheloid layers have the greatest intensity beneath areas of high eddy kinetic energy (Gardner, Richardson, & Mishonov, 2018; Gardner, Richardson, Mishonov, & Biscaye, 2018; Gardner et al., 2016). The low intensity of nepheloid layers in the deep Arctic basins suggests that currents and eddy kinetic energy are often not strong enough to resuspend sediment there.

6. Conclusions

Particle distributions in the Arctic are affected by currents, stratification, ice coverage and thickness, nutrient and light availability, and biological processes. The combination of c_p (a proxy for PM and POC) sections plotted with salinity, temperature, and Chl-*a* adds a background and baseline across the entire Arctic Ocean that is useful in deciphering some of the particle dynamics of the Arctic. The high vertical and horizontal resolution of the particle distribution using optical data in the sections compiled here and paired with particle composition on filtered samples through the whole water column, paints a vivid picture of particle distribution and sources. However, this is just a 2-month snapshot in a single year and there are undoubtedly seasonal and spatial changes in addition to climatological changes, especially the increase in ice-free areas, that need to be further documented seasonally and inter-annually to monitor and detect critical changes in biogeochemical processes.

Much of the Barents Sea has no seasonal ice cover. Strong winds during winter storms quickly cool the relatively warm, salty Atlantic water, some of which cascades down into these small basins, eroding sediment along the way. Optically derived PM concentrations in surface waters in the Barents Sea, Nansen Basin, and Chukchi Shelf are up to eight times greater than in most of the Canada Basin. On the Chukchi Shelf, abundant Chl-*a* was present in the regions of high c_p . Intermediate nepheloid layers with high c_p and low Chl-*a* on the shelf and upper slope between about 50 and 100 m, reveal shelf/slope transport into the Canada basin. The elevated c_p signal down to the base of the lower Pacific halocline water might be at least partly derived from lateral transport from the shelf/slope.

Chlorophyll maxima usually occur in surface waters, but Subsurface Chl-*a* Maxima (SCM) have been seen regularly in the Arctic Ocean. We observed SCMs of varying intensity between about 30 and 70 m depth, most notably in the Beaufort Gyre where the maximum Chl-*a* reached 1.5 μM . Ra-228 can be carried from the Chukchi Shelf into the Canada Basin and can include nutrients from shelf pore waters. That can help create SCMs when nutrient-rich waters (nitrate >0.5 μM) exist within the euphotic zone. An anomalous SCM was observed near the pole. We suggest that the water and components carried by the Trans Polar Drift are likely involved with this SCM.

The tight match between Chl-*a* contours and c_p suggests a correlation of c_p with biomass concentrations in the surface waters. Conversely, the high values of c_p near the sides or bottom of small basins in the Barents Sea show no Chl-*a*, so those high c_p values are most likely due to lithogenic sediment being resuspended by cascading of cold, hypersaline water.

River-borne and shelf sediment can be moved into the Arctic basins by shelf-edge currents, eddies, and fluctuating currents in submarine canyons. Most of the fine sediment moved seaward settles out within a few tens to a hundred kilometers from the margins, but some can spread much further into the basins as intermediate nepheloid layers. Another source of intermediate nepheloid layers could be Barrow Canyon.

Nepheloid layers based on c_p are weaker at the bottom of Canada and Amundsen basins than Barents Sea, but are manifest by near-bottom increases in c_p or an increase in pAl derived from aluminosilicate minerals in resuspended sediments. Based on correlations between c_p and other parameters, c_p is more sensitive to changes in POC than in PM.

Benthic nepheloid layers are detected in Arctic basins by both optical and chemical measurements. Any near-bottom increase in lithogenic particle concentrations suggests that there must have been local resuspension of bottom sediments and/or transport of sediments resuspended elsewhere. However, the low intensity of nepheloid layers in the deep Arctic basins suggests that currents and eddy kinetic energy are often insufficient to resuspend sediment there. Areas with significant topography such as the Chukchi Borderland and the shallower Barents Sea basins have isolated benthic nepheloid layers, possibly due in part to cascading of dense water sinking during rapid cooling of surface waters. Coupling optical measurements with large-volume in situ filtration provides a powerful combination of techniques to better understand sources, sinks and dynamics of particles throughout the water column.

Data Availability Statement

Supportive cooperation was provided by many personnel from the SIO Ocean Data Facility for USCGC Healy hydrographic data and by Benjamin Rabe from Alfred Wegener Institute for R/V Polarstern hydrographic data (PANGAEA data sets: Schauer (2016, http://doi.org/10.2312/BzPM_0703_2016), Rabe et al. (2016a, <https://doi.org/10.1594/PANGAEA.859559>, 2016b, <https://doi.org/10.1594/PANGAEA.859558>)). USCGC Healy transmissometer, fluorometer and hydrographic data are available through CCHDO expocode 33HQ20150809 and through Ocean Data View, Gardner et al. (2020, <https://odv.awi.de/en/data/ocean/global-transmissometer-database/>). All size-fractionated particle concentration and composition data described above are available on the Biological and Chemical Oceanography Data Management Office website Lam (2020, <https://www.bco-dmo.org/dataset/807340>).

Acknowledgments

The authors thank the captains and crews of USCGC Healy and R/V Polarstern plus chief scientists David Kadko, William Landing, and all science personnel aboard the USCGC Healy and chief scientist Ursula Schauer and all science personnel on the R/V Polarstern for collecting data during the joint GEOTRACES 2015 Arctic expeditions. Carl Lamborg and Angelique White are thanked for collecting and analyzing the pigments using HPLC. The authors thank Reiner Schlitzer for development of Ocean Data View software that we use for data analyses and figure compilations. Reviewers are thanked for their suggestions and questions that helped us improve the manuscript. Analysis and synthesis of these data have been supported by: U.S. National Science Foundation (contract OCE-1536565 to Gardner and Richardson; OCE-1535854 to Lam), NOAA (Grant NA19NES4320002 to Mishonov at Cooperative Institute for Satellite Earth System Studies -CISESS) at the University of Maryland/ESSIC and NCEI/NOAA (both U.S.), and support from the TAMU Earl F. Cook Professorship (Gardner).

References

- Aagaard, K., & Roach, A. T. (1990). Arctic Ocean-shelf exchange measurements in barrow canyon. *Journal of Geophysical Research*, *95*, 18163–18175. <https://doi.org/10.1029/jc095ic10p18163>
- Aksenov, Y., Ivanov, V. V., Nurser, A. G., Bacon, S., Polyakov, I. V., Coward, A. C., et al. (2011). The Arctic circumpolar boundary current. *Journal of Geophysical Research*, *116*, C09017. <https://doi.org/10.1029/2010JC006637>
- Ardyna, M., Babin, M., Gosselin, M., Devred, E., Belanger, S., Matsuoka, A., & Tremblay, J.-E. (2013). Parameterization of vertical chlorophyll-*a* in the Arctic Ocean: Impact of the subsurface chlorophyll maximum on regional, seasonal, and annual primary production estimates. *Biogeosciences*, *10*, 4383–4404. <https://doi.org/10.5194/bg-10-4383-2013>
- Armi, L. (1978). Mixing in the deep ocean—The importance of boundaries. *Oceanus*, *21*, 14–19.
- Armitage, T. W. K., Bacon, S., Ridout, A. L., Petty, A. A., Wolbach, S., & Tsamados, M. (2017). Arctic Ocean geostrophic circulation 2003–2014. *The Cryosphere Discussions*, *2017*, 1–32.
- Baker, E. T., & Lavelle, J. W. (1984). The effect of particle size on the light attenuation coefficient of natural suspensions. *Journal of Geophysical Research*, *89*, 8197–8203. <https://doi.org/10.1029/jc089ic05p08197>
- Bidigare, R. R., Van Heukelem, L., & Trees, C. C. (2005). Analysis of algal pigments by high-performance liquid chromatography. In R. A. Andersen (Ed.), *Algal culturing techniques* (pp. 327–345). Academic Press.
- Bishop, J. K. B., & Wood, T. J. (2008). Particulate matter chemistry and dynamics in the twilight zone at VERTIGO ALOHA and K2 sites. *Deep Sea Research Part 1*, *55*, 1684–1706.
- Boss, E., Guidi, L., Richardson, M. J., Stemann, L., Gardner, W., Bishop, J. K. B., et al. (2015). Optical techniques for remote and in situ characterization of particles pertinent to GEOTRACES. *Progress in Oceanography*, *133*, 43–54. <https://doi.org/10.1016/j.pocean.2014.09.007>
- Boss, E., Slade, W. H., Behrenfeld, M., & Dall'Olmo, G. (2009). Acceptance angle effects on the beam attenuation in the ocean. *Optics Express*, *17*, 1535–1550.
- Brewer, P. G., Spencer, D. W., Biscaye, P. E., Hanley, A., Sachs, P. S., Smith, C. L., et al. (1976). The distribution of particulate matter in the Atlantic Ocean. *Earth and Planetary Science Letters*, *32*, 393–402.
- Cacchione, D. A., & Drake, D. E. (1986). Nepheloid layers and internal waves over continental shelves and slopes. *Geo-Marine Letters*, *6*, 147–152. <https://doi.org/10.1007/BF02238085>
- Cai, P., Rutgers van der Loeff, M., Stimac, I., Nöthig, E.-M., Lepore, K., & Moran, S. B. (2010). Low export flux of particulate organic carbon in the central Arctic Ocean as revealed by ²³⁴Th/²³⁸U disequilibrium. *Journal of Geophysical Research*, *115*, C10037. <https://doi.org/10.1029/2009JC005595>
- Charette, M. A., Kipp, L. E., Jensen, L. T., Dabrowski, J. S., Whitmore, L. M., Fitzsimmons, J. N., et al. (2020). The Transpolar Drift as a source of riverine and shelf-derived trace elements to the central Arctic Ocean. *Journal of Geophysical Research, Oceans*, *125*(5), 1–34. <https://doi.org/10.1029/2019JC015920>
- Codispoti, L. A., Kelly, V., Thessen, A., Matrai, P., Suttles, S., Hill, V., et al. (2013). Synthesis of primary production in the Arctic Ocean: III. Nitrate and phosphate based estimates of net community production. *Progress in Oceanography*, *110*, 126–150. <https://doi.org/10.1016/j.pocean.2012.11.006>
- Corlett, W. B., & Pickart, R. S. (2017). The Chukchi slope current. *Progress in Oceanography*, *153*, 50–65.
- Cullen, J. J. (2015). Subsurface chlorophyll maximum layers: Enduring enigma or mystery solved? *Annual Reviews of Marine Science*, *7*, 207–239.
- Dmitrenko, I. A., Kirillov, S. A., Forest, A., Gratton, Y., Volkov, D. L., Williams, W. J., et al. (2016). Shelfbreak current over the Canadian Beaufort Sea continental slope: Wind-driven events in January 2005. *Journal of Geophysical Research: Oceans*, *121*, 2447–2468. <https://doi.org/10.1002/2015JC011514>

- Fetterer, F., Knowles, K., Meier, W. N., Savoie, M., & Windnagel, A. K. (2017). *Updated daily. Sea Ice Index, Version 3*. NSIDC: National Snow and Ice Data Center. <https://doi.org/10.7265/NSK072F8>
- Forest, A., Sampei, M., Hattori, H., Makabe, R., Sasaki, H., Fukuchi, M., et al. (2007). Particulate organic carbon fluxes on the slope of the Mackenzie Shelf (Beaufort Sea): Physical and biological forcing of shelf-basin exchanges. *Journal of Marine Systems*, 68, 39–54. <https://doi.org/10.1016/j.jmarsys.2006.10.008>
- Gardner, W. D. (1989). Periodic resuspension in Baltimore Canyon by focusing of internal waves. *Journal of Geophysical Research*, 94, 18185–18194.
- Gardner, W. D., Biscaye, P. E., Zaneveld, J. R. V., & Richardson, M. J. (1985). Calibration and comparison of the LDGO nephelometer and the OSU transmissometer on the Nova Scotian Rise. *Marine Geology*, 66, 323–344.
- Gardner, W. D., Mishonov, A. V., & Richardson, M. J. (2020). *Global Transmissometer Database V3* [Dataset]. <https://doi.org/10.13140/RG.2.2.36105.26724>
- Gardner, W. D., Richardson, M. J., & Mishonov, A. V. (2018). Global assessment of benthic nepheloid layers and linkage with upper ocean dynamics. *Earth and Planetary Science Letters*, 482, 126–134. <https://doi.org/10.1016/j.epsl.2017.11.008>
- Gardner, W. D., Richardson, M. J., Mishonov, A. V., & Biscaye, P. E. (2018). Global comparison of benthic nepheloid layers based on 52 yr of nephelometer and transmissometer measurements. *Progress in Oceanography*, 168, 100–111. <https://doi.org/10.1016/j.pocean.2018.09.008>
- Gardner, W. D., Southard, J. B., & Hollister, C. D. (1985). Sedimentation and resuspension in the western North Atlantic. *Marine Geology*, 65, 199–242.
- Gardner, W. D., Tucholke, B. E., Richardson, M. J., & Biscaye, P. E. (2016). Benthic storms, nepheloid layers, and linkage with upper ocean dynamics in the western North Atlantic. *Marine Geology*, 385, 304–327. <https://doi.org/10.1016/j.margeo.2016.12.012>
- Gardner, W. D., Walsh, I. D., & Richardson, M. J. (1993). Biophysical forcing of particle production and distribution during a spring bloom in the North Atlantic. *Deep Sea Research Part II: Topical Studies in Oceanography*, 40, 171–195.
- GEOTRACES Intermediate Data Product. (2021). <https://doi.org/10.5285/cf2d9ba9-d51d-3b7c-e053-8486abc0f5fd>
- Hedges, J., Baldock, J., Gélinais, Y., Lee, C., Peterson, M., & Wakeham, S. (2002). The biochemical and elemental compositions of marine plankton: A NMR perspective. *Marine Chemistry*, 78, 47–63. [https://doi.org/10.1016/S0304-4203\(02\)00009-9](https://doi.org/10.1016/S0304-4203(02)00009-9)
- Henley, S. F., Porter, M., Hobbs, L., Braun, J., Castel, R. G., Venables, E. J., et al. (2020). Nitrate supply and uptake in the Atlantic Arctic sea ice zone: Seasonal cycle, mechanisms, and drivers. *Philosophical Transactions of the Royal Society A*, 378, 20190361. <https://doi.org/10.1098/rsta.2019.0361>
- Honjo, S., Richard, A., Krishfield, R. A., Eglinton, T. I., Manganini, S. J., Kempa, J. N., et al. (2010). Biological pump processes in the cryope-lagic and hemipelagic Arctic Ocean: Canada Basin and Chukchi Rise. *Progress in Oceanography*, 85, 137–170.
- Hunkins, K. P. (1988). Mean and tidal currents in Baltimore Canyon. *Journal of Geophysical Research*, 93, 6917–6929.
- Hunkins, K. P., Thorndike, E. M., & Mathieu, G. (1969). Nepheloid layers and bottom currents in the Arctic Ocean. *Journal of Geophysical Research*, 74, 6995–7008.
- Hwang, J., Kim, M., Manganini, S. J., McIntyre, C. P., Haghipour, N., Park, J. J., et al. (2015). Temporal and spatial variability of particle transport in the deep Arctic Canada Basin. *Journal of Geophysical Research: Oceans*, 120, 2784–2799. <https://doi.org/10.1002/2014JC010643>
- Ivanov, V. V., Shapiro, G. I., Huthnance, J. M., Aleynik, D. L., & Golovin, P. N. (2004). Cascades of dense water around the world ocean. *Progress in Oceanography*, 60, 47–98.
- Jackson, J. M., Allen, S. E., Carmack, E. C., & McLaughlin, F. A. (2010). Suspended particles in the Canada Basin from optical and bottle data, 2003–2008. *Ocean Science*, 6, 799–813.
- Jensen, L. T., Morton, P., Twining, B. S., Heller, M. I., Hatta, M., Measures, C. I., et al. (2020). A comparison of marine Fe and Mn cycling: U.S. GEOTRACES GN01 western Arctic case study. *Geochimica et Cosmochimica Acta*, 288, 138–160. <https://doi.org/10.1016/j.gca.2020.08.006>
- Jones, E. P. (2001). Circulation in the Arctic Ocean. *Polar Research*, 20(2), 139–146.
- Jones, E. P., Swift, J. H., Anderson, L. G., Lipozer, M., Civitarese, G., Falkner, K. K., et al. (2003). Tracing Pacific water in the North Atlantic. *Journal of Geophysical Research*, 108(C4), 3116. <https://doi.org/10.1029/2001JC001141>
- Kadko, D., & Landing, W. (2015). U.S. Arctic GEOTRACES USCGC Healy (HLY1502) cruise report. Retrieved from https://www.bodc.ac.uk/resources/inventories/cruise_inventory/reports/healy1502.pdf
- Kadko, D., Pickart, R. S., & Mathis, J. (2008). Age characteristics of a shelf-break eddy in the western Arctic and implications for shelf-basin exchange. *Journal of Geophysical Research*, 113, C02018. <https://doi.org/10.1029/2007JC004429>
- Katlein, C., Arndt, S., Nicolaus, M., Perovich, K., Jakuba, M. L., Suman, S., et al. (2015). Influence of ice thickness and surface properties on light transmission through Arctic sea ice. *Journal of Geophysical Research: Oceans*, 120, 5932–5944. <https://doi.org/10.1002/2015JC010914>
- Kipp, L. E., Charette, M. A., Willard, S., Moore, W. S., Henderson, P. B., & Rigor, I. G. (2018). Increased fluxes of shelf-derived materials to the central Arctic Ocean. *Science Advances*, 4, eaao1302. <https://doi.org/10.1126/sciadv.aao1302>
- Kipp, L. E., Kadko, D. C., Pickart, R. S., Henderson, P. B., Moore, W. S., & Charette, M. A. (2019). Shelf-basin interactions and water mass residence times in the Western Arctic Ocean: Insights provided by radium isotopes. *Journal of Geophysical Research: Oceans*, 124, 3279–3297. <https://doi.org/10.1029/2019JC014988>
- Kipp, L. E., Spall, M. A., Pickart, R. S., Kadko, D. C., Moore, W. S., Dabrowski, J. S., & Charette, M. A. (2020). Observational and modeling evidence of seasonal trends in sediment-derived material inputs to the Chukchi Sea. *Journal of Geophysical Research: Oceans*, 125, e2019JC016007. <https://doi.org/10.1029/2019JC016007>
- Lam, P. J. (2020). *Size-fractionated major and minor particle composition and concentration from the from the U.S. GEOTRACES Arctic cruise (HLY1502) on USCGC Healy from August to October 2015*. Biological and Chemical Oceanography Data Management Office (BCO-DMO). (Version 1) Version Date 2020-04-01. <https://doi.org/10.26008/1912/bco-dmo.807340.1>
- Lam, P. J., Lee, J.-M., Heller, M. I., Mehic, S., Xiang, Y., & Bates, N. R. (2018). Size-fractionated distributions of suspended particle concentration and major phase composition from the U.S. GEOTRACES Eastern Pacific Zonal Transect (GP16). *Marine Chemistry*, 201, 90–107. <https://doi.org/10.1016/j.marchem.2017.08.013>
- Lam, P. J., Ohnemus, D. C., & Auro, M. E. (2015). Size-fractionated major particle composition and concentrations from the U.S. GEOTRACES North Atlantic Zonal transect. *Deep Sea Research Part II: Topical Studies in Oceanography*, 116, 303–320. <https://doi.org/10.1016/j.dsr2.2014.11.020>
- Lam, P. J., Twining, B. S., Jeandel, C., Roychoudhury, A. N., Resing, J. A., Santschi, P. H., & Anderson, R. F. (2015). Methods for analyzing the concentration and speciation of major and trace elements in marine particles. *Progress in Oceanography*, 133, 32–42. <https://doi.org/10.1016/j.pocean.2015.01.005>
- Landry, M. R., Brown, S. L., Campbell, L., Constantinou, J., & Lui, H. (1998). Spatial patterns in phytoplankton growth and microzooplankton grazing in the Arabian Sea during monsoon forcing. *Deep Sea Research Part II Topical Studies in Oceanography*, 45, 2353–2368.

- Lee, Z. P., Weidemann, A., Kindle, J., Arnone, R., Carder, K. L., & Davis, C. (2007). Euphotic zone depth: Its derivation and implication to ocean-color remote sensing. *Journal of Geophysical Research: Oceans*, *112*. <https://doi.org/10.1029/2006JC003802>
- Lorbacher, K., Dommenges, D., Niiler, P. P., & Köhl, A. (2006). Ocean mixed layer depth: A subsurface proxy of ocean-atmosphere variability. *Journal of Geophysical Research: Oceans*, *111*, C7. <https://doi.org/10.1029/2003JC002157>
- Marra, J. F., Lance, V. P., Vaillancourt, R. D., & Hargreaves, B. R. (2014). Resolving the ocean's euphotic zone. *Deep Sea Research Part I: Oceanographic Research Papers*, *83*, 45–50. <https://doi.org/10.1016/j.dsr.2013.09.005>
- Mathis, J. T., Pickart, R. S., Hansell, D. A., Kadko, D., & Bates, N. R. (2007). Eddy transport of organic carbon and nutrients from the Chukchi Shelf: Impact on the upper halocline of the western Arctic Ocean. *Journal of Geophysical Research*, *112*, C05011. <https://doi.org/10.1029/2006JC003899>
- McCave, I. N. (1986). Local and global aspects of the bottom nepheloid layers in the world ocean. *Netherlands Journal of Sea Research*, *20*(2/3), 167–181.
- Miller, M. C., McCave, I. N., & Komar, P. D. (1977). Threshold of sediment motion under unidirectional currents. *Sedimentology*, *24*, 507–527.
- Mishonov, A. V., Gardner, W. D., & Richardson, M. J. (2003). Remote sensing and surface POC concentration in the South Atlantic. *Deep Sea Research II*, *50*(22–26), 2997–3015. <https://doi.org/10.1016/j.dsr2.2003.07.007>
- Mountain, D. G., Coachman, L. K., & Aagaard, K. (1976). On the flow through Barrow Canyon. *Journal of Physical Oceanography*, *6*, 461–470.
- Mundy, C., Gosselin, M., Ehn, J., Gratton, Y., Rossnagel, A., Barber, D. G., et al. (2009). Contribution of under-ice primary production to an ice-edge upwelling phytoplankton bloom in the Canadian Beaufort Sea. *Geophysical Research Letters*, *36*, L17601. <https://doi.org/10.1029/2009GL038837>
- Nelson, C. D., & Creager, J. S. (1977). Displacement of Yukon-derived sediment from Bering Sea to Chukchi Sea during Holocene time. *Geology*, *5*, 141–146.
- Nikolopoulos, A., Pickart, R. S., Fratantoni, P. S., Shimada, K., Torres, D. J., & Jones, E. P. (2009). The western Arctic boundary current at 152°W: Structure, variability, and transport. *Deep Sea Research Part II: Topical Studies in Oceanography*, *56*(17), 1164–1181.
- O'Brien, M. C., Melling, H., Pedersen, T. F., & Macdonald, R. W. (2013). The role of eddies on particle flux in the Canada Basin of the Arctic Ocean. *Deep Sea Research Part I: Oceanographic Research Papers*, *71*, 1–20. <https://doi.org/10.1016/j.dsr.2012.10.004>
- Ober, S., Rijkenberg, M., & Gerringa, L. (2016a). Physical oceanography measured with ultra clean CTD/Water sampler-system during POLARSTERN cruise PS94 (ARK-XXIX/3). Retrieved from <https://www.tib.eu/de/suchen/id/datacite:10.1594%252FPANGAEA.859560/>
- Ober, S., Rijkenberg, M., & Gerringa, L. (2016b). Physical oceanography measured on water bottle samples with ultra clean CTD/Water sampler-system during POLARSTERN cruise PS94 (ARK-XXIX/3). <https://www.tib.eu/de/suchen/id/datacite:doi~10.1594%252FPANGAEA.859561>
- Peralta-Ferriz, C., & Woodgate, R. A. (2015). Seasonal and interannual variability of pan-arctic surface mixed layer properties from 1979 to 2012 from hydrographic data, and the dominance of stratification for multiyear mixed layer depth shoaling. *Progress in Oceanography*, *134*, 19–53.
- Perovich, D., Meier, W., Tschudi, M., Farrell, S., Hendricks, S., Gerland, S., et al. (2019). Sea ice cover. In “state of the climate in 2018”. *Bulletin of the American Meteorological Society*, *100*(9), S146–S150.
- Pickart, R. S. (2004). Shelfbreak circulation in the Alaskan Beaufort Sea: Mean structure and variability. *Journal of Geophysical Research*, *109*, C04024. <https://doi.org/10.1029/2003JC001912>
- Puig, P., Greenan, B. J. W., Li, M. Z., Prescott, R. H., & Piper, D. J. W. (2013). Sediment transport processes at the head of Halibut Canyon, Eastern Canada margin: An interplay between internal tides and dense shelf-water cascading. *Marine Geology*, *341*, 14–28.
- Rabe, B., Schauer, U., Ober, S., Horn, M., Hoppmann, M., Korhonen, M., et al. (2016a). *Physical oceanography measured on water bottle samples during POLARSTERN cruise PS94 (ARK-XXIX/3)*. Alfred Wegener Institute, Helmholtz Centre for Polar and Marine Research. <https://doi.org/10.1594/PANGAEA.859559>
- Rabe, B., Schauer, U., Ober, S., Horn, M., Hoppmann, M., Korhonen, M., et al. (2016b). *Physical oceanography during POLARSTERN cruise PS94 (ARK-XXIX/3)*. Alfred Wegener Institute, Helmholtz Centre for Polar and Marine Research. <https://doi.org/10.1594/PANGAEA.859558>
- Roach, A. T., Aagaard, K., Pease, C. H., Salo, S. A., Weingartner, T., Pavlov, V., & Kulakov, M. (1995). Direct measurement of transport and water properties through the Bering Strait. *Journal of Geophysical Research*, *100*(C9), 18443–18457.
- Roesler, C., Uitz, J., Claustre, H., Boss, E., Xing, X., Organelli, E., et al. (2017). Recommendations for obtaining unbiased chlorophyll estimates from in situ chlorophyll fluorometers: A global analysis of WET Labs ECO sensors. *Limnology and Oceanography: Methods*, *15*(2017), 572–585. <https://doi.org/10.1002/lom3.10185>
- Rudels, B., Jones, E. P., Schauer, U., & Eriksson, P. (2004). Atlantic sources of the Arctic Ocean surface and halocline waters. *Polar Research*, *23*(2), 181–208. <https://doi.org/10.3402/polar.v23i2.6278>
- Rutgers van der Loeff, M., Kipp, L., Charette, M. A., Moore, W. S., Black, E., Stimac, I., et al. (2018). Radium isotopes across the Arctic Ocean show time scales of water mass ventilation and increasing shelf inputs. *Journal of Geophysical Research: Oceans*, *123*, 4853–4873. <https://doi.org/10.1029/2018JC013888>
- Schauer, U., & The Expedition PS94 of the Research Vessel POLARSTERN to the central Arctic Ocean in 2015 (2016). *Reports on polar and marine research* (Vol. 703, p. 170). Alfred Wegener Institute for Polar and Marine Research. https://doi.org/10.2312/BzPm_0703_2016
- Schlitzer, R. (2020). Ocean data view. Retrieved from <https://odv.awi.de>
- Seidov, D., Antonov, J. I., Arzayus, K. M., Baranova, O. K., Biddle, M., Boyer, T. P., et al. (2015). Oceanography north of 60°N from world ocean database. *Progress in Oceanography*, *132*, 153–173. <https://doi.org/10.1016/j.pocean.2014.02.003>
- Slagter, H. A., Reader, H. E., Rijkenberg, M. J. A., Rutgers van der Loeff, M., Baar, H. J. W. D., & Gerringa, L. J. A. (2017). Organic Fe speciation in the Eurasian Basins of the Arctic Ocean and its relation to terrestrial DOM. *Marine Chemistry*, *197*, 11–25.
- Spall, M. A., Pickart, R. S., Fratantoni, P. S., & Plueddemann, A. J. (2008). Western Arctic Shelfbreak eddies: Formation and transport, 2008. *Journal of Physical Oceanography*, *38*, 1644–1668.
- Spall, M. A., Pickart, R. S., Li, M., Itoh, M., Lin, P., Kikuchi, T., & Qi, Y. (2018). Transport of Pacific water into the Canada Basin and the formation of the Chukchi slope current. *Journal of Geophysical Research: Oceans*, *123*, 7453–7471. <https://doi.org/10.1029/2018JC013825>
- Springer, A. M., & Mcroy, C. P. (1993). The paradox of pelagic food webs in the northern Bering Sea—III. Patterns of primary production. *Continental Shelf Research*, *13*(5–6), 575–599. [https://doi.org/10.1016/0278-4343\(93\)90095-F](https://doi.org/10.1016/0278-4343(93)90095-F)
- Steele, M., Morison, J., Ermold, W., Rigor, I., Ortmeyer, M., & Shimada, K. (2004). Circulation of summer Pacific halocline water in the Arctic Ocean. *Journal of Geophysical Research: Oceans*, *109*, C02027. <https://doi.org/10.1029/2003JC002009>
- Steiner, N., Sou, T., Deal, C., Jackson, J. M., Jin, M., Popova, E., et al. (2016). The future of the subsurface chlorophyll-*a* maximum in the Canada Basin—A model intercomparison. *Journal of Geophysical Research: Oceans*, *121*(1), 387–409. <https://doi.org/10.1002/2015JC011232>
- Strom, S. L. (1993). Production of pheopigments by marine protozoa: Results of laboratory experiments analyzed by HPLC. *Deep Sea Research Part I*, *40*, 57–80. [https://doi.org/10.1016/0967-0637\(93\)90053-6](https://doi.org/10.1016/0967-0637(93)90053-6)
- Taylor, S. R., & McLennan, S. M. (1995). The geochemical evolution of the continental crust. *Reviews of Geophysics*, *33*(2), 241–265. <https://doi.org/10.1029/95RG00262>

- Thorndike, E., & Ewing, M. (1967). Photographic nephelometers for the deep sea, Chap. 10. In J. B. Hersey (Ed.), *Deep-sea photography* (Vol. 1967, pp. 113–116). Johns Hopkins Press.
- Timmermans, M.-L., & Marshall, J. (2020). Understanding Arctic Ocean circulation: A review of ocean dynamics in a changing climate. *Journal of Geophysical Research: Oceans*, *125*, e2018JC014378. <https://doi.org/10.1029/2018JC014378>
- Toole, J. M., Timmermans, M.-L., Perovich, D. K., Krishfield, R. A., Proshutinsky, A., & Richter-Menge, J. A. (2010). Influences of the ocean surface mixed layer and thermohaline stratification on Arctic sea ice in the central Canada Basin. *Journal of Geophysical Research*, *115*, C10018. <https://doi.org/10.1029/2009JC005660>
- Tremblay, J.-E., Simpson, K., Martin, J., Miller, L., Gratton, Y., Barber, D., & Price, N. M. (2008). Vertical stability and the annual dynamics of nutrients and chlorophyll fluorescence in the coastal, southeast Beaufort Sea. *Journal of Geophysical Research*, *113*, C07S90. <https://doi.org/10.1029/2007JC004547>
- Turnewitsch, R., Falahat, S., Nycander, J., Dale, A., Scott, R. B., & Furnival, D. (2013). Deep-sea fluid and sediment dynamics—Influence of hill-to seamount-scale seafloor topography. *Earth-Science Reviews*(127), 203–241. <https://doi.org/10.1016/j.earscirev.2013.10.005>
- Watanabe, E., Onodera, J., Harada, N., Honda, M. C., Kimoto, K., Kikuchi, T., et al. (2014). Enhanced role of eddies in the Arctic marine biological pump. *Nature Communications*, *5*, 3950. <https://doi.org/10.1038/ncomms4950>
- Woodgate, R. A., Aagaard, K., Thomas, J., & Weingartner, T. J. (2005). A year in the physical oceanography of the Chukchi Sea: Moored measurements from autumn 1990–1991. *Deep Sea Research II*, *52*, 3116–3149.
- Xiang, Y., & Lam, P. J. (2020). Size-fractionated compositions of marine suspended particles in the western Arctic Ocean: Lateral and vertical sources. *Journal of Geophysical Research: Oceans*, *125*, e2020JC016144. <https://doi.org/10.1029/2020JC016144>